

## Holographic evolution of the mutual information

---

**Andrea Allais and Erik Tonni**

*Center for Theoretical Physics, Massachusetts Institute of Technology,  
Cambridge, MA 02139, U.S.A.*

*E-mail:* [a\\_allais@mit.edu](mailto:a_allais@mit.edu), [tonni@mit.edu](mailto:tonni@mit.edu)

**ABSTRACT:** We compute the time evolution of the mutual information in out of equilibrium quantum systems whose gravity duals are Vaidya spacetimes in three and four dimensions, which describe the formation of a black hole through the collapse of null dust. We find the holographic mutual information to be non monotonic in time and always monogamous in the ranges explored. We also find that there is a region in the configuration space where it vanishes at all times. We show that the null energy condition is a necessary condition for both the strong subadditivity of the holographic entanglement entropy and the monogamy of the holographic mutual information.

**KEYWORDS:** AdS-CFT Correspondence, Black Holes, Holography and condensed matter physics (AdS/CMT)

**ARXIV EPRINT:** [1110.1607](https://arxiv.org/abs/1110.1607)

---

**Contents**

<b>1</b>	<b>Introduction</b>	<b>1</b>
<b>2</b>	<b>Holographic entanglement entropy for Vaidya geometries</b>	<b>3</b>
2.1	Vaidya metrics	4
2.2	Holographic entanglement entropy	6
2.3	Three dimensional case and thin shell limit	10
<b>3</b>	<b>Holographic mutual information</b>	<b>12</b>
3.1	Limiting regimes in three dimensions	17
<b>4</b>	<b>Strong subadditivity and null energy condition</b>	<b>20</b>
<b>5</b>	<b>Holographic tripartite information and monogamy</b>	<b>22</b>
<b>6</b>	<b>Conclusions</b>	<b>26</b>

---

**1 Introduction**

Entanglement entropy is a measure of the quantum entanglement in systems with many degrees of freedom which has been object of intense investigation in condensed matter, quantum information and quantum gravity.

Given a system whose total Hilbert space  $H$  can be written as a direct product  $H = H_A \otimes H_B$  and whose state is characterized by the density matrix  $\rho$ , one can define the reduced density matrix  $\rho_A \equiv \text{Tr}_B \rho$  by tracing over the degrees of freedom of  $B$ . Then, the entanglement entropy  $S_A$  is the corresponding Von Neumann entropy  $S_A = -\text{Tr}_A(\rho_A \log \rho_A)$ . The situation mostly studied in the literature is when  $A$  is given by a spatial region and  $B$  is its complement. In this case the entanglement entropy is also called geometric entropy and  $S_A$  behaves according to an *area law*: in  $d > 1$  spatial dimensions we have  $S_A \propto \text{Area}(\partial A)/\epsilon^{d-1} + \dots$ , where  $\epsilon$  is the UV cutoff of the theory and the dots represent terms of higher order in  $\epsilon$  [1]. In two spacetime dimensions the divergence is logarithmic and more quantitative analysis has been performed for conformal field theories, where the symmetry provides powerful computational techniques. For these theories, when  $A$  is given by an interval of length  $\ell$  in an infinite line and the temperature is zero, we have the famous result  $S_A = (c/3) \log(\ell/\epsilon) + c'_1$ , where  $c$  is the central charge and  $c'_1$  is a constant [2–4] (see [5] for a recent review). The most useful method to get  $S_A$  is the so called *replica trick*, which consists in computing the Renyi entropies  $S_A^{(n)} \equiv (1 - n)^{-1} \log \text{Tr} \rho_A^n$  for integer  $n$ . The entanglement entropy is then obtained as  $S_A = -\partial_n \text{Tr} \rho_A^n |_{n=1}$ .

For quantum field theories with a holographic dual, the prescription to compute  $S_A$  in the boundary theory through a bulk computation has been conjectured in [6, 7] for static backgrounds and then generalized to stationary and time dependent geometries in [8] (see [9] for a review). The proposal of [6, 7] satisfies many properties and also important inequalities of the entanglement entropy (the simplest of them is the strong subadditivity) [10–12]. Nevertheless, a proof for this formula is not known [13, 14].

Interesting insights in the structure of entanglement can be obtained by considering two disjoint regions, namely  $A = A_1 \cup A_2$  with  $A_1 \cap A_2 = \emptyset$  [15–18]. In this case the most interesting quantity to study is the mutual information  $I(A_1, A_2) \equiv S_{A_1} + S_{A_2} - S_{A_1 \cup A_2}$ , which has the nice property that the leading divergence due to the area law cancels. The Renyi mutual information has been analytically computed for some simple two dimensional conformal field theories like the free compactified boson [17] and the Ising model [18], and it has been shown that it encodes all the data of the theory (all the conformal dimensions of the primaries and their correlation functions) in contrast with the entanglement entropy of a single interval which contains only the central charge. Unfortunately, the analytic continuation that allows to obtain  $I(A_1, A_2)$  is not known in general but only in some limiting regimes. Detailed studies of  $I(A_1, A_2)$  for spin chain models have also been done [19–22].

The holographic formula of [6, 7] for static backgrounds has been applied for disjoint regions [14, 23, 24] and a qualitative disagreement with respect to the expectations from the simple two dimensional conformal field theories mentioned above has been found. Indeed the holographic mutual information displays a continuous transition with discontinuous first derivative from zero to positive values as the two regions get closer. This could be explained through the fact that the holographic formula holds for large  $c$  and it should be corrected in order to recover the results obtained for the models whose central charges are of the order one. Nevertheless the holographic formula of [6, 7] and its generalization for time dependent backgrounds [8] are believed to be correct for large  $c$  and we will employ this prescription in our analysis.

The entanglement entropy is a very important quantity to study in order to understand the physics out of equilibrium and the processes of thermalization. In particular, one is interested in the unitary time evolution of the entanglement entropy when the system starts from a state which is not an eigenstate of the Hamiltonian of the system. This occurs for instance when a system is prepared in an eigenstate of the corresponding Hamiltonian and suddenly a tunable parameter of the Hamiltonian (e.g. the magnetic field) is changed (*global quench*). Then the system evolves unitarily accordingly with the new Hamiltonian starting from a state which is not one of its eigenstates. Another interesting situation is when the system is prepared in the ground state of two decoupled parts which are joined together at  $t = 0$  and then the whole system unitarily evolves through the translationally invariant Hamiltonian (*local quench*). These situations have been studied for two dimensional systems by employing conformal field theory techniques and spin chains models [25–29]. Nevertheless, there are still many open problems. For instance, contrary to what happens for classical systems [30, 31], the renormalization procedure is not well understood when the translation invariance in the time direction is broken.

Thermalization processes have also been widely considered from the holographic point of view (see [32] for a review). For instance, the holographic counterpart of the unitary evolution of a system towards a stationary state is a gravitational collapse whose final state is a black hole. In this process both the initial and the final states are thermal and the holographic entanglement entropy can be computed through the prescription of [8].

The Vaidya metrics (see e.g. [33]) are simple backgrounds realizing this setup, but there are also alternative holographic models [34, 35]. They are solutions of the Einstein equations with negative cosmological constant and a non trivial energy momentum tensor containing a mass function, constrained by the null energy condition, which describe the formation of a black hole through the collapse of a shell of null dust. The null geodesics in these geometries have been studied in [36] but here we are interested in the spacelike ones, which occur in the computation of the holographic entanglement entropy [8, 37, 38]. The Vaidya metrics are simplifications of more general models considered e.g. in [39] (tensionful shell) and [40]. Other holographic thermalization setup have also been studied [34]. The study of the holographic entanglement entropy in Vaidya backgrounds is usually numerical but recently an analytic computation has been done for the limiting regime of thin shell in three spacetime dimensions [41, 42]. We will largely employ this result in our analysis because it allows to explore a larger range of parameters. The holographic analysis of the two point functions in these dynamical geometries has been carried out in [41–43].

In this paper we study the holographic entanglement entropy in three and four dimensional Vaidya backgrounds. In section 2 we introduce the metrics and the corresponding holographic entanglement entropy for a single region in the boundary theory. In section 3 we study the holographic mutual information and its transition curves in the configuration space. In section 4 we explore the relation between the null energy condition for the Vaidya metrics and the strong subadditivity for the holographic entanglement entropy. In section 5 we extend the analysis performed in the previous sections to the holographic tripartite information in order to verify the monogamy of the holographic mutual information in Vaidya spacetimes and study how this property is influenced by the null energy condition.

**Note added.** While we were completing the writing of this paper, [44] appeared and it has a substantial overlap with our results.

## 2 Holographic entanglement entropy for Vaidya geometries

In this section we introduce the Vaidya metrics in  $d+1$  dimensions (subsection 2.1) and we describe some known results about the holographic entanglement entropy in these backgrounds (subsection 2.2). In subsection 2.3 we focus on the three dimensional case because it is the simplest to study and some analytical results have recently been found [41, 42] which will be widely employed in the remaining part of the paper.

## 2.1 Vaidya metrics

The  $d + 1$  dimensional Vaidya metrics in Poincaré coordinates read

$$ds^2 = \frac{l^2}{z^2} \left[ - (1 - m(v)z^d) dv^2 - 2dzdv + d\vec{x}^2 \right] \quad (2.1)$$

(we set  $8\pi G_N^{(d+1)} = 1$ ) where  $\vec{x} = \{x_1, \dots, x_{d-1}\}$  are the spatial boundary coordinates. The Ricci scalar of (2.1) is  $R = -(d + 1)d/l^2$ . The metric (2.1) is a solution of the Einstein equations in presence of matter

$$G_{\mu\nu} + \Lambda g_{\mu\nu} = T_{\mu\nu} \quad \Lambda = -\frac{d(d-1)}{2l^2} \quad (2.2)$$

where the energy momentum tensor has only one non vanishing component

$$T_{vv} = \frac{d-1}{2} z^{d-1} \partial_v m(v) . \quad (2.3)$$

The metric (2.1) describes the formation of a black hole through the collapse of null dust, which is characterized by the  $T_{\mu\nu}$  just introduced. It is important to observe that the translational invariance along the directions contained in  $\vec{x}$  is preserved at any time. This is a key feature of the setup characterizing global quenches in the boundary theory.

In processes of gravitational collapse, it is not yet understood how to characterize the formation of a black hole through local time evolution. To this purpose, some generalizations of the concept of horizon have been proposed, and, in our backgrounds we can distinguish between two horizons, the event and the apparent horizon [45–47]. The apparent horizon is the boundary of the trapped surfaces associated to a given foliation. For the metrics (2.1) a foliation which preserves the translation invariance in the directions of  $\vec{x}$  is given by  $v = \text{const}$  and  $z = \text{const}$ . The location of the apparent horizon of (2.1) reads [8, 37]

$$z_a = \frac{1}{m(v)^{1/d}} . \quad (2.4)$$

Instead, the event horizon is given by

$$\frac{dz_e}{dv} = -\frac{1 - m(v)z_e^d}{2} . \quad (2.5)$$

When the mass profile  $m(v)$  is constant  $m(v) = M$ , the metric (2.1) describes the geometry of the Schwarzschild black hole with planar horizon. This can be clearly seen through the following change of coordinates

$$v = t + p(z) \quad p'(z) = -\frac{1}{1 - Mz^d} \quad (2.6)$$

which allows to write (2.1) as

$$ds^2 = \frac{l^2}{z^2} \left[ -(1 - Mz^d) dt^2 + \frac{dz^2}{1 - Mz^d} + d\vec{x}^2 \right] \quad (2.7)$$

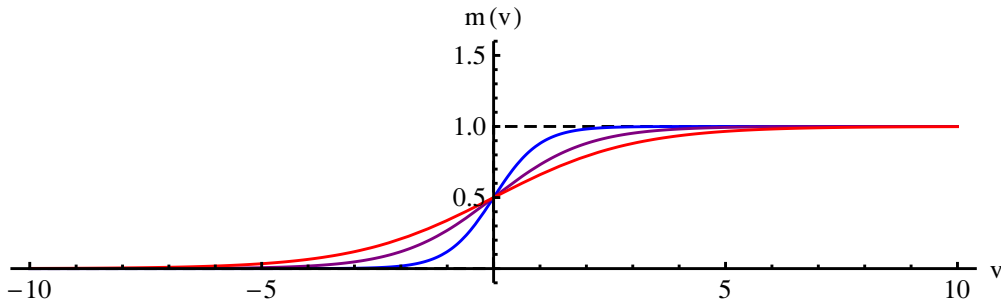


**Figure 1.** The function (2.9) for different values of the thickness  $a_v$  and  $M = 1$ . The dashed curve is a step function and corresponds to the limiting regime of thin shell  $a_v \rightarrow 0$ .

i.e. the usual form for a Schwarzschild black hole of mass  $M$  in the Poincaré coordinates. For  $l = 1$  the Hawking temperature of this black hole is given by  $T_H = dM^{1/d}/(4\pi)$ . It is also straightforward to check that for  $m(v) = 0$  identically the metric (2.1) describes  $\text{AdS}_{d+1}$  in the Poincaré coordinates

$$ds^2 = \frac{l^2}{z^2}(-dt^2 + dz^2 + d\vec{x}^2) \quad t = v + z. \quad (2.8)$$

This tells us that the Vaidya metric (2.1) is asymptotically  $\text{AdS}_{d+1}$ .

The formation of the Schwarzschild black hole (2.7) from  $\text{AdS}_{d+1}$  is described by considering a function  $m(v)$  which interpolates between 0 and the finite value  $M > 0$  in an strictly increasing way. The profile for  $m(v)$  is usually chosen to be

$$m(v) = M \frac{1 + \tanh(v/a_v)}{2}. \quad (2.9)$$

Given this  $m(v)$ , the metric (2.1) describes a background which evolves from pure planar  $\text{AdS}_{d+1}$  at early times to Schwarzschild black brane with mass  $M$  at late times because of an infalling shell of null dust. The parameter  $a_v$  determines the time scale of the transition between these two regimes, since it parameterizes the thickness of the shell which falls along  $v = 0$ . The mass function (2.9) is shown in figure 1. In the limiting case  $a_v \rightarrow 0$ , the mass profile  $m(v)$  becomes a step function  $M\theta(v)$  and the infalling shell describes a shock wave. This limit is very interesting because it captures the essential physics of the problem and one can hope to find analytic solutions for the quantities considered. For the holographic entanglement entropy in three spacetime dimensions this has been done in [41, 42] and we will largely employ this result.

An important inequality to impose on the energy momentum tensor  $T_{\mu\nu}$  in (2.2) to guarantee the positivity of the energy density is the *null energy condition*, namely  $T_{\mu\nu}N^\mu N^\nu \geq 0$  for any null vector  $N^\mu$  [45, 46]. This inequality has been employed to study the  $c$  theorems from the holographic point of view [48, 49] and their generalizations in presence of boundaries [50–53]. For the energy momentum tensor (2.3), imposing the null energy condition means

$$\partial_v m(v) \geq 0 \quad (2.10)$$

which is clearly satisfied by the profile (2.9). In section 4 and 5 we consider mass profiles violating this condition and the effect of this violation on the holographic entanglement entropy.

## 2.2 Holographic entanglement entropy

For static spacetimes like  $\text{AdS}_{d+1}$  (2.8) and the Schwarzschild black hole (2.7), the prescription to obtain the entanglement entropy  $S_A = -\text{Tr}(\rho_A \log \rho_A)$  in the boundary theory through a holographic computation in the bulk has been proposed in [6, 7]. It reads

$$S_A = \frac{\text{Area}(\gamma_A)}{4G_N^{(d+1)}} \tag{2.11}$$

where  $G_N^{(d+1)}$  is the Newton constant for the  $d + 1$  dimensional bulk and  $\gamma_A$  is defined as the *minimal* surface among the spatial ones which extend into the bulk and share the boundary with  $A$ , i.e.  $\partial\gamma_A = \partial A$  ( $\gamma_A$  is homologous to  $A$ ). Thus,  $\gamma_A$  is a codimension two surface living on the  $t = \text{const}$  slice and has minimal area. Since  $\gamma_A$  lives in an asymptotically  $\text{AdS}_{d+1}$  space and it reaches its boundary, placed at  $z = 0$  in the Poincaré coordinates,  $\text{Area}(\gamma_A)$  is infinite and therefore it must be regularized by introducing a small cutoff  $\epsilon > 0$  in the holographic direction, namely the restriction  $z > \epsilon$  is imposed during the bulk computation. The series expansion of  $S_A$  in  $\epsilon$  depends on  $d$ , and one of the first checks of (2.11) was that this expansion reproduces in the holographic way the leading UV divergence of the entanglement entropy as computed in field theory with other methods. In particular, for  $d > 2$ , the leading divergence of  $S_A$  is proportional to  $\text{Area}(\partial A)/\epsilon^{d-2}$ , with a non universal coefficient [1] (this is the so called *area law*). For  $d = 2$ , when the boundary CFT is two dimensional and the spatial region  $A$  is a segment of length  $\ell$  (thus  $\partial A$  is made by two points), the entanglement entropy  $S_A$  diverges logarithmically with a universal coefficient given by the central charge of the theory [2–4]. Besides these fundamental checks, it has been shown that the holographic proposal (2.11) satisfies the strong subadditivity condition [11] and other more complicated inequalities characterizing the entanglement entropy [12], which will be discussed in section 4 and 5.

The proposal (2.11) for static backgrounds has been generalized to time dependent geometries in [8]. In these cases  $S_A$  is still given by (2.11) but with  $\gamma_A$  obtained as an *extremal* surface, namely as the saddle point of the proper area functional. This proposal is covariantly well defined and reduces to the previous one when the spacetime is static. Let us explain it in details for the Vaidya  $d + 1$  dimensional spacetimes (2.1).

We consider as  $d - 1$  dimensional spatial region  $A$  in the boundary theory a rectangular strip parameterized by  $x_1 \in (-\ell/2, \ell/2)$  and  $x_2, \dots, x_{d-1} \in (0, \ell_\perp)$ , at fixed value of the boundary time coordinate  $t$ . This choice is less symmetric than the case of  $A$  given by a ball, but a crucial simplification occurs in this case.

According to the proposal of [8], the holographic entanglement for this spatial region  $A$  is given by the area of the extremal surface  $\gamma_A$  whose profile is most conveniently specified by  $v \equiv v(x_1)$  and  $z \equiv z(x_1)$  (we are assuming that  $\gamma_A$  is translationally invariant in the other boundary coordinates  $x_2, \dots, x_{d-1}$  parameterizing  $A$ ), with the following boundary conditions

$$v(-\ell/2) = v(\ell/2) = t \qquad z(-\ell/2) = z(\ell/2) = 0. \tag{2.12}$$

With these boundary conditions, the boundary of  $\gamma_A$  coincides with the boundary of  $A$  along the boundary temporal evolution. Since  $x_1$  is the relevant independent variable, we

will denote it by  $x$  in the following. The area of such *spacelike* surface (thus the determinant of the induced metric under the square root must be taken with the positive sign) is given by the following functional

$$\text{Area}(\gamma_A) \equiv \mathcal{A}_d \equiv l^{d-1} 2\ell_{\perp}^{d-2} \int_0^{\frac{\ell}{2}} \frac{1}{z^{d-1}} \sqrt{1 - [1 - m(v)z^d](v')^2 - 2v'z'} dx \quad (2.13)$$

where  $' \equiv d/dx$  and where we exploit the fact that  $z(x)$  and  $v(x)$  are symmetric under reflection about a plane, which we take to be  $x = 0$ . This consideration about parity determines the factor 2 and the integration extrema in (2.13).

The area functional (2.13) is the one we have to extremize in order to get the codimension two surface  $\gamma_A$  and hence to compute the holographic entanglement entropy for the time dependent Vaidya spaces through (2.11) [8]. In other words,  $\gamma_A$  is the solution to the two equations of motion of (2.13). Since the integrand in (2.13) does not contain  $x$  explicitly, we have the following conservation equation

$$\left(\frac{z_*}{z}\right)^{2(d-1)} = 1 - [1 - m(v)z^d](v')^2 - 2v'z' \quad (2.14)$$

where  $z_* = z(0)$  is the maximum value of  $z(x)$ , which is characterized by  $z' = v' = 0$ . This conservation law is what makes the rectangular shape of  $A$  simpler than the circular one. The two equations of motion obtained by minimizing the functional (2.13) read

$$[1 - m(v)z^d]v'' + z'' - \frac{\partial_v m(v)}{2} z^d (v')^2 - d m(v) z^{d-1} z' v' = 0 \quad (2.15)$$

$$z v'' - \frac{d-2}{2} m(v) z^d (v')^2 + (d-1)[(v')^2 + 2v'z' - 1] = 0. \quad (2.16)$$

By taking the derivative w.r.t.  $x$  of the conservation equation (2.14) and using one of these two equations of motion, one obtains the other one. Thus, it is sufficient to consider only (2.14) and e.g. (2.16) to find  $v(x)$  and  $z(x)$ .

Given a solution  $(v(x), z(x))$  of the equations of motion, its area can be computed by evaluating the integral (2.13) on it. Using (2.14), this area can be written as follows

$$\mathcal{A}_d = l^{d-1} 2\ell_{\perp}^{d-2} \int_0^{\frac{\ell}{2}} \frac{z_*^{d-1}}{z^{2(d-1)}} dx. \quad (2.17)$$

As discussed above, this integral is divergent because the spacetime we are dealing with, being asymptotically  $\text{AdS}_{d+1}$ , is non compact and the spatial surface  $\gamma_A$  we are considering reaches its boundary (see the boundary conditions (2.12)).

The divergence of  $\mathcal{A}_d$  can be obtained by studying the same problem in  $\text{AdS}_{d+1}$  in the standard way [7]. Subtracting this divergence we obtain the finite term of the area which is the main quantity we are interested in. For  $d > 2$  we have

$$\mathcal{A}_{d,\text{reg}} \equiv 2l^{d-1} \ell_{\perp}^{d-2} \lim_{\eta \rightarrow 0^+} \left( \int_0^{\frac{\ell}{2}-\eta} \frac{z_*^{d-1}}{z^{2(d-1)}} dx - \frac{1}{(d-2) e^{d-2}} \right) \equiv l^{d-1} \ell_{\perp}^{d-2} L_{d,\text{reg}} \quad (2.18)$$

---

<sup>0†</sup>In all the plots of this paper the numerical values of the parameter characterizing the different curves are evenly spaced.



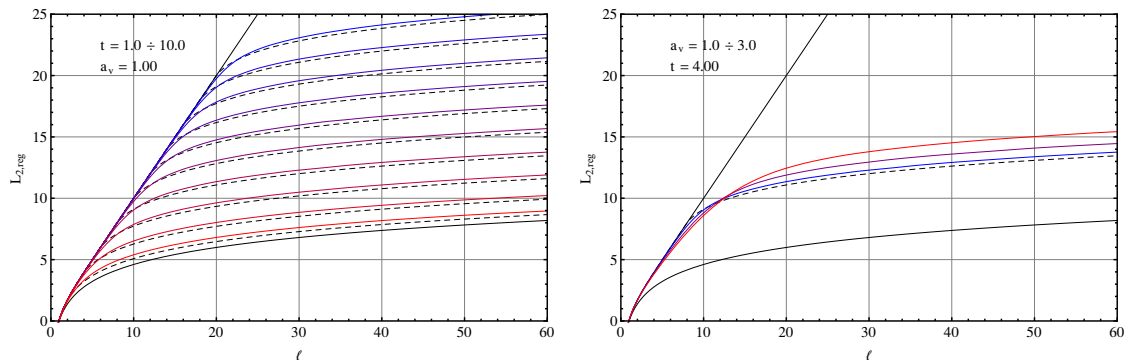


**Figure 2.** Finite term of the holographic entanglement entropy for the Vaidya metric in three dimensions (see (2.11) and (2.18) up to a factor), with  $m(v)$  given by (2.9) [8, 37]. On the left,  $L_{2,\text{reg}}(\ell, t)$  for different values<sup>†</sup> of boundary time  $t$ , increasing from the red curve to the blue one, at a fixed value of  $a_v$ . On the right,  $L_{2,\text{reg}}(\ell, a_v)$  at a fixed value of  $t$  and different values of the thickness  $a_v$ , which increases going from the blue curve to the red one. In both plots, the black curves correspond to the limiting regimes of  $\text{AdS}_3$  (bottom curve, from (2.24)) and of the BTZ black hole (top curve, from (2.24)), while the dashed curves are in the thin shell limit  $a_v = 0$ .

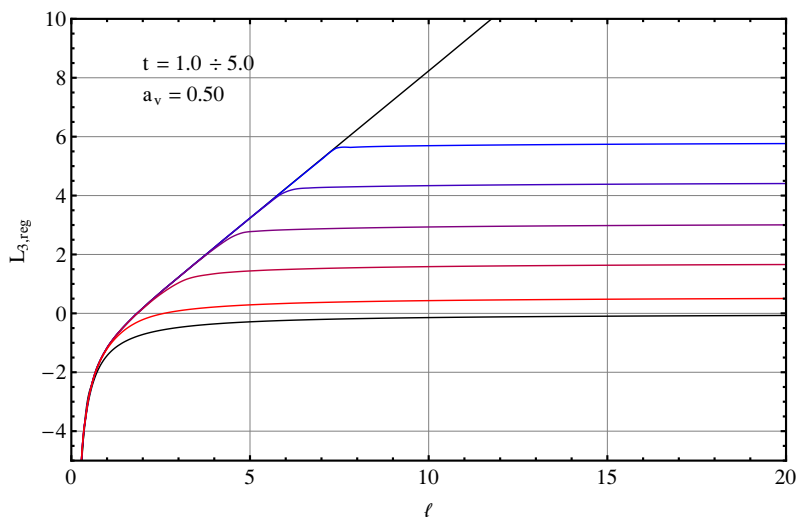


**Figure 3.** Finite term of the holographic entanglement entropy for the Vaidya metric in four dimensions (proportional to  $L_{3,\text{reg}}(\ell, t)$ ), with  $m(v)$  given by (2.9), fixed  $a_v$  and different boundary times  $t$ , increasing from the red curve to the blue one. The black curves correspond to the limiting regimes of  $\text{AdS}_4$  (bottom curve from (2.20)) and of the Schwarzschild black hole in four dimensions (top curve).

where  $\epsilon \equiv z(\ell/2 - \eta)$  is the UV cutoff in the boundary theory. Notice that in this case we need to subtract just one diverging term to regularize  $\mathcal{A}_d$ . This is a feature of the strip; indeed when the region  $A$  is a circle there are more terms to subtract to make the area finite [7].

In order to find the solution of (2.14) and (2.16) satisfying the boundary conditions (2.12), first we exploit the reflection symmetry about  $x = 0$  and solve the Cauchy problem whose initial conditions are given by

$$z(0) = z_* \quad v(0) = v_* . \tag{2.19}$$

Then, we shoot in the variables  $z_*$ ,  $v_*$  to impose (2.12).<sup>1</sup> It turns out that the points at which the solution reaches the boundary become increasingly sensitive to the initial conditions and to the accuracy of the integration as either  $d$  or  $\ell$  increase. As a consequence, it becomes more and more difficult to impose (2.12). This technical difficulty limits the range of parameters we are able to explore for  $d > 2$ . Once the solution is found, the implementation of the numerical integration and limit in (2.18) is quite straightforward.

In figure 2 and 3 we show respectively  $L_{2,\text{reg}}$  (three dimensional Vaidya) and  $L_{3,\text{reg}}$  (four dimensional Vaidya) as functions of  $\ell$  and for different values of the two other important parameters involved in our problem: the boundary time  $t$  and the thickness of the shell  $a_v$ . The three dimensional case deserves a separated discussion (see subsection 2.3) because it is the simplest situation and therefore some analytic results can be found [41, 42]. Notice that the main qualitative features of the plots in figure 2 and 3 are independent of the number of dimensions. The black curves represent the limiting regimes, which are  $\text{AdS}_{d+1}$  in the early times (bottom curve) and the  $d + 1$  dimensional Schwarzschild black hole at late times (top curve). For generic  $d > 2$  the result for  $\text{AdS}_{d+1}$  is known [7]

$$L_{d,\text{reg}} \Big|_{\text{AdS}_{d+1}} = -\frac{(2\sqrt{\pi})^{d-1}}{d-2} \left[ \frac{\Gamma(\frac{d}{2(d-1)})}{\Gamma(\frac{1}{2(d-1)})} \right]^{d-1} \frac{1}{\ell^{d-2}}. \quad (2.20)$$

Unfortunately  $L_{d,\text{reg}}$  for the  $d + 1$  dimensional Schwarzschild black hole is not known. Very few analytic results are available for minimal surfaces in four and higher dimensional black holes but the curves for  $L_{d,\text{reg}}$  have been studied [24, 54].

At any intermediate, finite and fixed boundary time  $t$  during the black hole formation, we can observe from figure 2 and 3 that  $L_{d,\text{reg}}(\ell, t)$  goes over the Schwarzschild black hole curve for small  $\ell$  and, at some point (which depends on  $t$ ), it leaves from it to adopt an  $\text{AdS}_{d+1}$  like behavior shifted vertically. Indeed, at any finite time, the shell is fixed in some region of the bulk, and we have  $\text{AdS}_{d+1}$  geometry inside the shell and a Schwarzschild black hole outside, with the thickness of the transient region proportional to  $a_v$ . For small values of  $\ell$ , the extremal surface stays completely outside the shell, and far from it. Therefore it feels only the Schwarzschild black hole geometry. As  $\ell$  increases, the extremal surface begins to extend in the region inside the shell, and therefore to feel the  $\text{AdS}_{d+1}$  part of the geometry. This makes  $L_{d,\text{reg}}$  deviate from the Schwarzschild behavior. When  $\ell$  is very large, a big part of the extremal surface is inside the shell and therefore its length is determined by  $\text{AdS}_{d+1}$ , explaining the asymptotic behavior of the curves in figure 2 and 3 for large  $\ell$ . The vertical shift in this regime is due to the part of the surface which is close to the boundary: being outside the shell, it feels the Schwarzschild black hole geometry and it provides a larger contribution to  $L_{d,\text{reg}}$  than the  $\text{AdS}_{d+1}$  geometry. From the plot on the right in figure 2, we can observe that, as the thickness  $a_v$  decreases,  $L_{d,\text{reg}}$  reproduces the Schwarzschild black hole result for a larger range of  $\ell$  and also that the vertical shift for large values of  $\ell$  w.r.t. the  $\text{AdS}_{d+1}$  curve decreases.

---

<sup>1</sup>This approach is different from the one used in [37], where shooting takes place from the boundary. We favored shooting from  $x = 0$  because it is a regular point of the solution  $(v(x), z(x))$ .

At this point we find it useful to have a look to the shape of the extremal surfaces, which is shown in figure 4 for the case of two disjoint regions in the boundary, and will be studied in section 3. The extremal surfaces go backward in the bulk time direction  $v$  and, around  $v = 0$ , they penetrate into the shell, probing the  $\text{AdS}_{d+1}$  geometry inside [37].

### 2.3 Three dimensional case and thin shell limit

The three dimensional Vaidya geometry ( $d = 2$ ) is the simplest situation and consequently very useful study, in order to get some physical intuition and more analytical results [8, 37, 41, 42] that will be helpful in the higher dimensional case. Moreover, the CFT on the boundary theory is two dimensional, and the powerful methods developed for these class of models lead to important results [2–4], which are very helpful to test the holographic techniques.

For a two dimensional boundary theory, the region  $A$  is simply a one dimensional segment of length  $\ell$  at fixed boundary time  $t$ . The extremal surface we are looking for is given by the geodesic connecting the two extrema of this segment and extending in the bulk. The Vaidya geometry (2.1) for  $d = 2$  interpolates between  $\text{AdS}_3$  in Poincaré coordinates and the BTZ black hole of [55]. By employing  $r \equiv 1/z$  as holographic coordinate, the equations (2.14) and (2.16) become respectively [8, 37]

$$\frac{r^4}{r_*^2} = -[r^2 - m(v)](v')^2 + 2r'v' + r^2 \quad (2.21)$$

and

$$r v'' - 2r'v' + r^2[(v')^2 - 1] = 0. \quad (2.22)$$

The first important feature of the three dimensional case is the leading divergence in the expansion of the entanglement entropy  $S_A$ , which is not power like but logarithmical [2–4]. Roughly, this could be justified by observing that in the two dimensional boundary theory there is no “area law” behavior because the  $\partial A$  is made by two points and it has null measure. In three dimensions the regularized area (2.18) coincides with the regularized length of the geodesic

$$L_{2,\text{reg}} \equiv \lim_{\eta \rightarrow 0^+} \left( 2 \int_0^{\frac{\ell}{2} - \eta} \frac{z_*}{z^2} dx + 2 \log \epsilon \right) \quad \epsilon \equiv z(\ell/2 - \eta) \quad (2.23)$$

where  $\epsilon > 0$  is the UV cutoff of the holographic direction. The limiting regimes at early and late times are respectively  $\text{AdS}_3$  (bottom black curve in figure 2) and BTZ (top black curve), whose regularized lengths read [6, 7]

$$L_{2,\text{reg}} \Big|_{\text{AdS}_3} = 2 \log \ell \quad L_{2,\text{reg}} \Big|_{\text{BTZ}} = 2 \log \left[ \frac{\beta_H}{\pi} \sinh \left( \frac{\pi \ell}{\beta_H} \right) \right] \quad (2.24)$$

where  $\beta_H \equiv 1/T_H = 2\pi/\sqrt{M}$  for  $l = 1$ . By employing the well known Brown-Henneaux central charge  $c = 3l/(2G_N^{(3)})$  [56] for asymptotically  $\text{AdS}_3$  spaces and the lengths (2.24) for the geodesics in  $\text{AdS}_3$  and in the BTZ black hole, in [6, 7] it was checked that the holographic prescription (2.11) reproduces the expressions for the entanglement entropy of

a single interval of length  $\ell$  in a two dimensional CFT with central charge  $c$  defined on an infinite line at  $T = 0$  and  $T > 0$  respectively [2–4]

$$S_A \Big|_{T=0} = \frac{c}{3} \log \left( \frac{\ell}{\epsilon} \right) \qquad S_A \Big|_{T>0} = \frac{c}{3} \log \left[ \frac{\beta}{\pi\epsilon} \sinh \left( \frac{\pi\ell}{\beta} \right) \right]. \quad (2.25)$$

Here  $\beta \equiv 1/T$  and the second expression in (2.25) reduces to the first one when  $\beta \rightarrow +\infty$ , as expected. The same happens in (2.24) for  $M \rightarrow 0$ .

Besides AdS<sub>3</sub> and the BTZ black hole, there is another limiting regime of the Vaidya background in three dimensions where the holographic entanglement entropy has been computed analytically [41, 42]: the *infinitely thin shell limit*, defined as the case in which the thickness of the shell vanishes  $a_v \rightarrow 0$ . In this limit the metric is (2.1), with the mass profile given by a step function  $m(v) = M\theta(v)$  at  $v = 0$ , the non vanishing component  $T_{vv}$  of the energy-momentum tensor is proportional to a delta function  $\delta(v)$  and the infalling shell represents a shock wave. The resulting geometry is given by a planar black brane (a BTZ black hole with a planar horizon) outside the shock wave and an AdS<sub>3</sub> region inside the shock wave. The geodesics in both these regimes are known analytically. The geodesics entering inside the shell in the full shock wave geometry are piecewise curves made by joining the BTZ geodesic outside the shell with the AdS<sub>3</sub> geodesic inside. The actual prescription for joining them is described in [41, 42].

The length of these geodesics is then given by the sum of the three pieces: the first one going from one extremum of  $A$  to the shell in the BTZ geometry, the second one inside the shell connecting two junction points of the shell at the same  $z$  but different  $x$  (AdS<sub>3</sub>) and a third one going from this other point of the shell to the other extremum of  $A$  on the boundary, again in the BTZ geometry (see figure 4).

Denoting by  $r_H$  the position of the horizon of the BTZ geometry outside the shell, the regularized length of the geodesics entering into the shell can be written as [41, 42]

$$L_{2,\text{reg}} \Big|_{\text{thin shell}} = 2 \log \left( \frac{\sinh(r_H t)}{r_H s(\ell, t)} \right) \quad (2.26)$$

where the function  $s = s(\ell, t) \equiv \sin \theta \in [0, 1]$  with  $\theta \in [0, \pi/2]$  can be extracted from

$$\ell = \frac{1}{r_H} \left[ \frac{2 \cos \theta}{\rho \sin \theta} + \log \left( \frac{2(1 + \cos \theta)\rho^2 + 2\rho \sin \theta - \cos \theta}{2(1 + \cos \theta)\rho^2 - 2\rho \sin \theta - \cos \theta} \right) \right] \quad (2.27)$$

with  $\rho$  defined as follows

$$\rho \equiv \frac{1}{2} \left( \coth(r_H t) + \sqrt{\coth^2(r_H t) - \frac{2 \cos \theta}{1 + \cos \theta}} \right). \quad (2.28)$$

In order to plot  $L_{2,\text{reg}}$  as function of  $\ell$  and of the boundary time  $t$ , we need both  $L_{2,\text{reg}}|_{\text{BTZ}}$  (2.24) and  $L_{2,\text{reg}}|_{\text{thin shell}}$  (2.26). In fact, for small values of  $\ell$  the geodesic is outside the shell and  $L_{2,\text{reg}}$  is given by  $L_{2,\text{reg}}|_{\text{BTZ}}$ . As  $\ell$  increases, at some point the geodesic enters into the shell and for  $\ell$  larger than this value  $L_{2,\text{reg}}$  is given by  $L_{2,\text{reg}}|_{\text{thin shell}}$ . From (2.27)

one can observe that, for any fixed boundary time  $t$ , the function  $\ell$  decreases as  $\theta$  goes from 0 to  $\pi/2$ . Thus, the critical value of  $\ell$  from which we have to start using  $L_{2,\text{reg}}|_{\text{thin shell}}$  is

$$\ell|_{\theta=\pi/2} = \frac{1}{r_H} \log \left( \frac{\rho|_{\theta=\pi/2} + 1}{\rho|_{\theta=\pi/2} - 1} \right) = \frac{1}{r_H} \log \left( \frac{\coth(r_H t) + 1}{\coth(r_H t) - 1} \right) = 2t. \quad (2.29)$$

Given a boundary time  $t$ , this is the value of  $\ell$  after which the geodesic enters into the shell. In figure 2, the  $a_v = 0$  limit we are discussing is represented by the dashed curves. The relation (2.29) can be checked on those plots, since the dashed curve characterized by  $t$  deviates from the BTZ continuous black curve at  $\ell = 2t$ . This is the relation found in [25] for two dimensional CFT models between the duration of the linear increasing of the entanglement entropy after a global quench and the size  $\ell$  of the spatial interval  $A$ , which lead the authors to suggest the quasiparticles picture.

### 3 Holographic mutual information

In this section we consider the holographic mutual information for three and four dimensional Vaidya metrics, employing also the analytic solution for the thin shell limit of the three dimensional case. We numerically compute its dependence from the size and the distance of the strips and also study the transition curves in the configuration space, finding that a time independent region exists where the holographic mutual information vanishes at all times.

When the boundary region  $A$  we are interested in is made by two disjoint regions  $A = A_1 \cup A_2$  with  $A_1 \cap A_2 = \emptyset$ , the situation becomes more complicated and also more interesting. The most important quantity to consider in this case is the mutual information

$$I(A_1, A_2) \equiv S_{A_1} + S_{A_2} - S_{A_1 \cup A_2} \quad (3.1)$$

because in this linear combination the leading divergence due to the area law cancels. The quantity  $I(A_1, A_2)$  measures the classical and quantum correlation between  $A_1$  and  $A_2$ .

Within the context of two dimensional CFT, the Renyi entropies  $S_{A_1 \cup A_2}^{(n)} \equiv (1 - n)^{-1} \log \text{Tr} \rho_{A_1 \cup A_2}^n$  (for interger  $n \geq 2$ ) have been computed for the free compactified boson [17] and for the Ising model [18]. These results have been checked against existing numerical data on spin chains [16, 20]. Unfortunately, the analytic continuation of these quantities for  $n \rightarrow 1$ , which is needed to find the mutual information through derivation  $S_{A_1 \cup A_2} = -\partial_n \text{Tr} \rho_{A_1 \cup A_2}^n|_{n=1}$ , is still unknown for the general expressions, but it has been done for some limiting regimes of the parameters like the decompactification regime for the free boson (when the field takes values on the whole real line) [17] or when the two intervals are very far apart [18]. The main quantitative lesson one learns from these results is that the Renyi entropies, or equivalently the Renyi mutual information  $I^{(n)}(A_1, A_2)$ , which is defined in the obvious way by combining the Renyi entropies as done in (3.1) for the mutual information, encodes all the data of the CFT. In other words,  $\text{Tr} \rho_{A_1 \cup A_2}^n$  does not contain only the central charge  $c$ , like  $S_A$  for one interval, but also all the conformal dimensions and all the OPE coefficients of the theory.

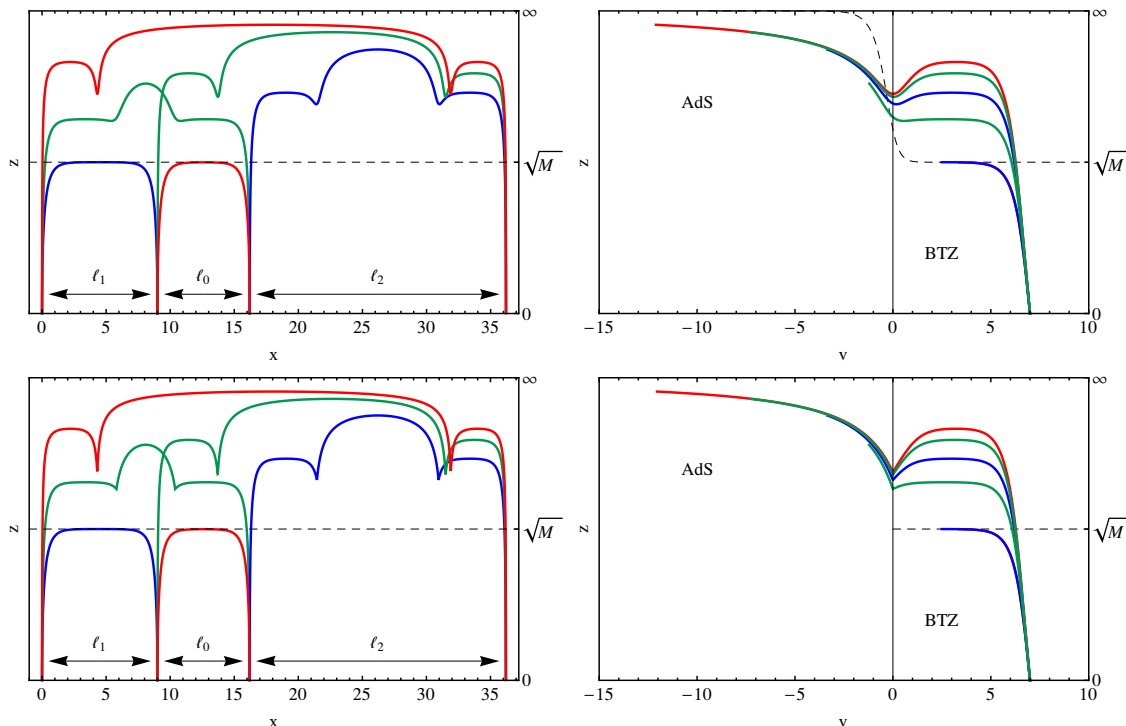


**Figure 4.** Geodesics configuration for the holographic mutual information at the transition point for three dimensional Vaidya geometry ( $d = 2$ ) with  $M = 1$  in (2.9). The total length of the geodesics for the connected configuration (red) and the disconnected one (blue) is the same. In the upper plots  $a_v = 0.5$  while in the bottom ones  $a_v \rightarrow 0$  (thin shell limit). The boundary time is  $t = 7$  (see the intersection of the curves with the horizontal axis in the plots on the right). The  $z$  axis has been compactified using the arctan function. The green geodesics represent the mixed configuration, which is suboptimal. Notice that they do not intersect, as can be clearly seen from the plot on the right, top line.

From the AdS/CFT point of view, it is natural to study the holographic mutual information, which is defined like in (3.1) with  $S_A$  given by the holographic formula (2.11), as a further test of the holographic prescription (2.11) for the entanglement entropy. It is known [14, 24] that the holographic mutual information displays a continuous transition from zero to positive values with a discontinuous first derivative which is not observed in the simple CFT models considered so far [17, 18]. This feature is believed to be a large  $c$  effect.

Given the two disconnected regions  $A_1$  and  $A_2$  in the boundary, there are three configurations of two surfaces extending in the bulk whose boundaries coincide with  $\partial A = \partial A_1 \cup \partial A_2$ : the first is simply the union of the two surfaces characterizing  $S_{A_1}$  and  $S_{A_2}$  (which bounds two disconnected volumes and hence it will be referred to as “disconnected” configuration). The second one is the “connected” configuration, given by a bridge connecting  $A_1$  and  $A_2$  through the bulk (bounding a single connected volume in the bulk). The third configuration is composed by the extremal surface connecting the first extrema of the regions (let us assume for the moment we have strips) and the one connecting the second ones. We will denote this case as “mixed” configuration. In this mixed configuration, for a

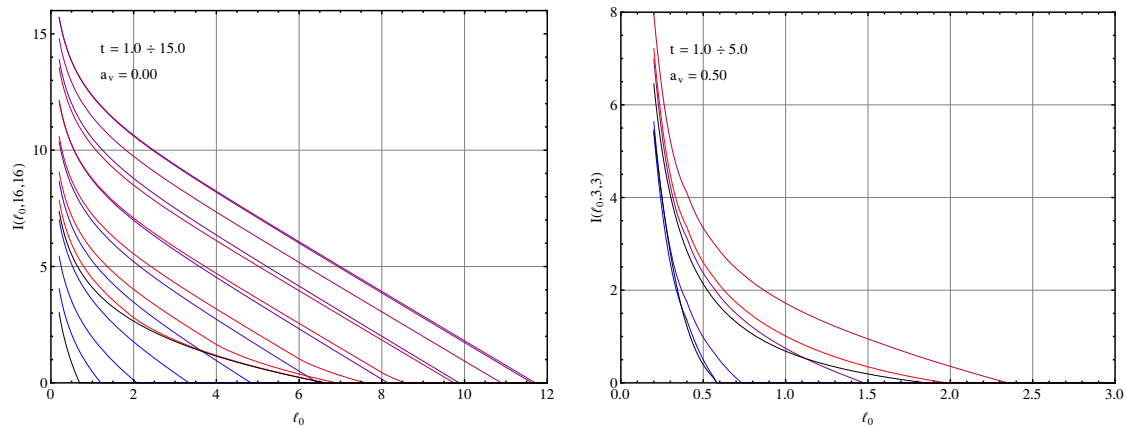


**Figure 5.** Holographic mutual information  $I(\ell_0, \ell_1, \ell_1)$  in terms of  $\ell_0$  for Vaidya metrics in three (plots on the left, infinitely thin shell regime) and four dimensions (plots on the right) in the bulk. Different curves are characterized by the boundary time  $t$ , whose value increases going from the red curves to the blue ones with  $\Delta t = 1$  and within the range indicated. The black curves correspond to  $\text{AdS}_{d+1}$  (top curve) and Schwarzschild black hole (bottom curve). The transition of the holographic mutual information is continuous with a discontinuous first derivative.

static background, the extremal surfaces intersect, but for a dynamical background this is not generally true (see the set of green geodesics in figure 4). Also, for two disjoint circular regions in a 2+1 dimensional boundary, this type configuration does not occur at all. A similar mixed configurations of surfaces also occurs in the proof of the strong subadditivity for the holographic entanglement entropy [11]. Since they do not always intersect for time dependent backgrounds, the proof cannot be extended to the dynamical case in a straightforward way. In our case, since  $\mathcal{A}_{d,\text{reg}}$  is an increasing function of the size of  $A$  at any fixed time  $t$  (see figure 2 and 3) we can claim that this mixed configuration is always suboptimal with respect to the disconnected one (see also the upper line of figure 13). Thus, the regularized area entering in the holographic computation of  $S_{A_1 \cup A_2}$  reads

$$\mathcal{A}_{d,\text{reg}} = \min\left(\mathcal{A}_{d,\text{reg}}|_{\text{connected}}, \mathcal{A}_{d,\text{reg}}|_{\text{disconnected}}\right). \tag{3.2}$$

Notice that both configurations display the same UV divergence which cancels in the linear combination (3.1). In three dimensional backgrounds ( $d = 2$ ), the lengths of the geodesics are involved in (3.2).

It is straightforward to notice that, when the disconnected configuration is minimal, the holographic mutual information is zero, while it is positive in the other case. Moreover, when  $A_1$  and  $A_2$  are very far apart from each other, the disconnected configuration is always minimal. Thus, considering a configuration space which describes all the possible sizes and the relative distance between  $A_1$  and  $A_2$ , there must be some region of this space where the “connected” configuration is minimal and some other region where, instead, the “disconnected” configuration is minimal. The corresponding holographic mutual information is zero and positive respectively. The curve in the configuration space which characterizes this transition in the configuration space is given by the following equation

$$\mathcal{A}_{d,\text{reg}}|_{\text{connected}} = \mathcal{A}_{d,\text{reg}}|_{\text{disconnected}}. \tag{3.3}$$



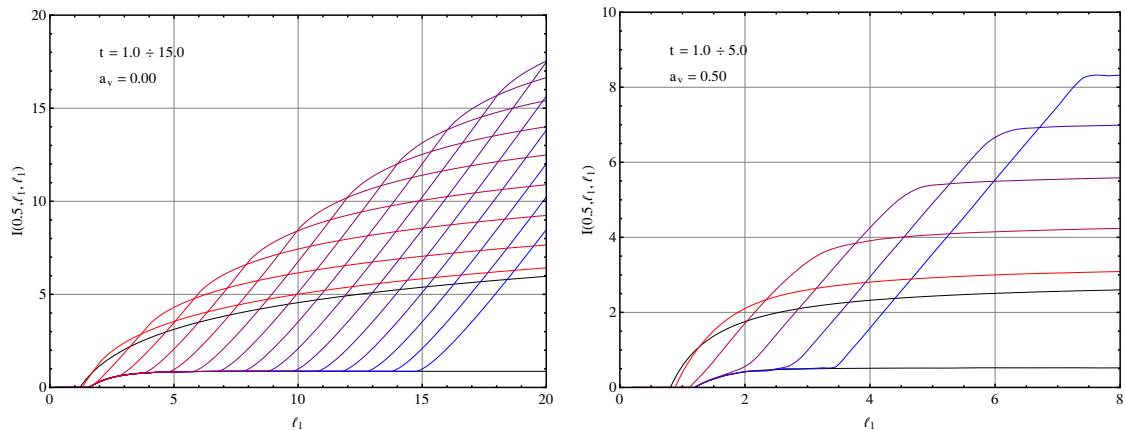


**Figure 6.** Holographic mutual information  $I(\ell_0, \ell_1, \ell_1)$  as function of  $\ell_1$  at fixed  $\ell_0$  for Vaidya metrics in three (plots on the left, infinitely thin shell regime) and four dimensions (plots on the right) in the bulk. The other parameters are the same ones employed in figure 5.

This equation is not easy to solve and must be studied case by case. The examples of  $\text{AdS}_{d+1}$  and of the charged black hole in four dimensions have been considered in [14, 24]. Here we study this equation for the Vaidya metrics (2.1) in three and four dimensions.

Let us first consider the holographic mutual information  $I(\ell_0, \ell_1, \ell_2)$  (see (3.1)) for the Vaidya metrics (2.1) in three and four dimensions with the mass profile given by (2.9). This quantity depends on many variables and our analysis is mainly numerical. We take equal strips  $\ell_2 = \ell_1$  for our plots unless indicated otherwise.

In figure 5 and 6 we show the dependence of  $I(\ell_0, \ell_1, \ell_1)$  from the distance  $\ell_0$  between the intervals and the size  $\ell_1$  respectively. The continuous black curves represent the corresponding quantities in the limiting regimes of  $\text{AdS}_{d+1}$  and Schwarzschild black hole (BTZ black hole in three dimensions), while the colored ones are characterized by intermediate boundary times, as indicated in the plot. Notice that the qualitative features of the curve do not change with the number of dimensions. In general we can clearly observe the transition of the mutual information from positive values to zero when  $\ell_0$  increases at fixed size  $\ell_1$  (figure 5) and from zero to positive values as  $\ell_1$  increases at fixed separation  $\ell_0$  (figure 6). This transition is continuous with a discontinuous first derivative and unfortunately we do not have a clear understanding of it. We recall that the holographic mutual information is positive when the connected configuration is favored. When we plot a family of curves parameterized by the boundary time  $t$ , the common feature one observes is that the bigger  $t$  is, the larger is the range of variables where the curve characterized by  $t$  reproduces the corresponding black hole result. Then, for any finite  $t$  at some point the curve deviates from the black hole behavior and tends asymptotically to the  $\text{AdS}_{d+1}$  behavior, shifted by a constant.

In three dimensions ( $d = 2$ ) we can take advantage of the fact that the exact solution is known in the thin shell limit  $a_v \rightarrow 0$  (see (2.26)) [41, 42] and working with the analytic solution allows us to extend the range of variables that we can explore.



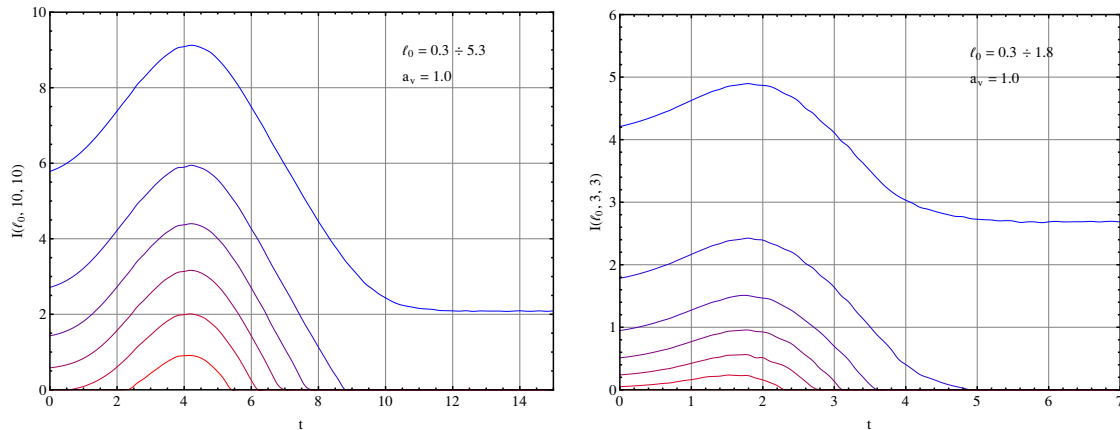


**Figure 7.** Holographic mutual information  $I(\ell_0, \ell_1, \ell_1)$  as function of the boundary time  $t$  at fixed  $\ell_1$ . The different curves are characterized by different values of  $\ell_0$  which increase going from the top curve to the bottom one. As in the previous figures, we show the  $d = 2$  case on the left and the  $d = 3$  case on the right. For a fixed value of  $\ell_1$ , varying  $\ell_0$  three different behaviors are observed.

As for the dependence on the boundary time  $t$  of the holographic mutual information  $I(\ell_0, \ell_1, \ell_1)$ , this is shown in figure 7 for different values of the separation  $\ell_0$  between the two strips and a fixed value of their size  $\ell_1$  in three dimensions (plot on the left) and in four dimensions (plot on the right). From these plots we observe that, at a fixed of  $\ell_1$ , varying the separation  $\ell_0$  between the strips four different behaviors are observed. For  $\ell_0$  very large  $I(\ell_0, \ell_1, \ell_1)$  is zero at all times. Decreasing  $\ell_0$  (i.e. going from the bottom to the top curves in figure 7) we find that  $I(\ell_0, \ell_1, \ell_1)$  is zero at  $t = 0$ , then it becomes positive for a finite range of  $t$  and then it vanishes again. Decreasing further  $\ell_0$  the holographic mutual information starts positive at  $t = 0$  but then it vanishes at some time. For even smaller  $\ell_0$ ,  $I(\ell_0, \ell_1, \ell_1)$  is positive for any boundary time  $t$ , that is, the connected configuration is always favored.

In order to describe these four regimes from another point of view, we find it useful to study the transition curve of  $I(\ell_0, \ell_1, \ell_2)$  in the configuration space given by  $\ell_2$ ,  $\ell_1$  and  $\ell_0$ . That is, we find the family of curves parameterized by  $t$  which solves the equation (3.3). These transition curves are shown in figure 8, 9 (three dimensional case) and 10 (four dimensional case).

We set  $\ell_2 = \omega \ell_1$  for some finite  $\omega > 0$  and then consider the space  $(\ell_1, \ell_0)$ . In figure 8 we display the three dimensional background for some  $a_v > 0$  and  $\omega = 1$ . In the plot on the right the  $a_v$  dependence is show at fixed  $t$ . The dashed curves correspond to the  $a_v \rightarrow 0$  limit and are obtained through the analytic solution of [41, 42]. The main feature we notice is that it is possible to draw a critical curve  $\hat{\ell}_0(\ell_1)$  which is *independent of the time*  $t$  such that for any configuration specified by a point above this curve the holographic mutual information is zero at all times. This critical curve is above the transition curve of  $\text{AdS}_3$  and it depends on  $a_v$ . The region below it and above the  $\text{AdS}_3$  transition curve becomes larger as  $a_v$  becomes smaller, as can be observed from the plot on the right in figure 8. In figure 9 we consider the transition curves for the analytic solution in the  $a_v \rightarrow 0$

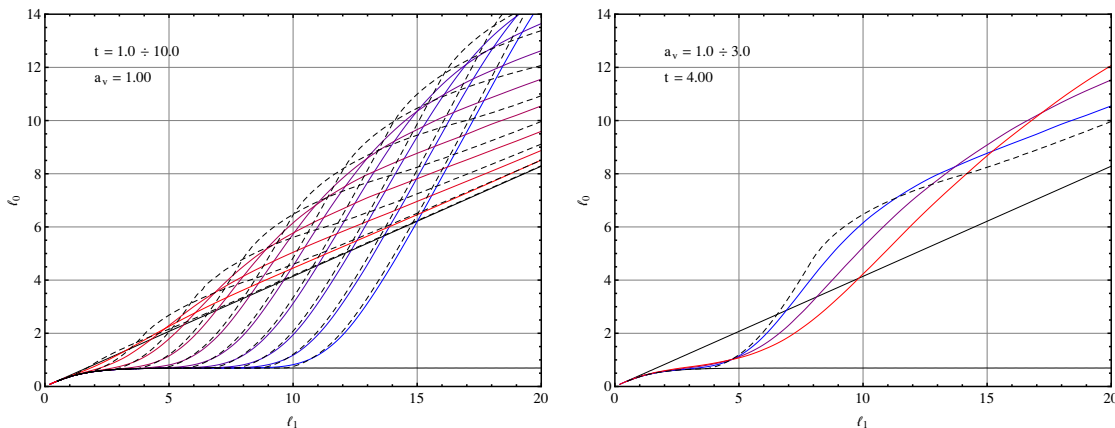


**Figure 8.** Transition point of the holographic mutual information  $I(\ell_0, \ell_1, \ell_1)$  for the three dimensional Vaidya metric in the configuration space  $(\ell_1, \ell_0)$ . The black curves represent the limiting regimes of  $\text{AdS}_3$  (top curve, given by (3.6) at  $\omega = 1$ ) and BTZ (bottom curve, given by (3.10) at  $\omega = 1$ ). On the left we plot the transition point for different times (increasing as we go from the red to the blue curve) and thickness  $a_v = 1$  (the dashed curves represent the thin shell limit  $a_v = 0$ ). On the right, the transition point in the configuration space is plotted at a fixed time  $t = 4$  for various values of the thickness  $a_v$  in (2.9): from  $a_v = 0$  (dashed curve) to  $a_v = 3$  (red curve). There is a whole region of the configuration space where the holographic mutual information is zero for any boundary time.

limit, in order to extend the range of the configuration space  $(\ell_1, \ell_0)$  and also to study the dependence on  $\omega$ , which is equal to 1 on the left and 2 on the right. Comparing the two plots we can clearly see the linear behavior of the critical curve for large  $\ell_1$  and notice that it depends also on  $\omega$ .

In figure 10 we consider the four dimensional background for  $\omega = 1$ : the qualitative features are the same described above, but numerical difficulties restrict the configuration space we are able to explore.

### 3.1 Limiting regimes in three dimensions

Here we discuss the analytic expressions of the transition curves for the limiting regimes of the black hole formation process in three dimensions, namely  $\text{AdS}_3$  for early times and the BTZ black hole in the late times (black curves in figure 5, 6, 8 and 9).

The boundary theory is two dimensional and the two spatial regions  $A_1$  and  $A_2$  at  $t = \text{const}$  are intervals whose lengths are respectively  $\ell_1 = x_{21}$  and  $\ell_2 = x_{43}$  (we adopt the notation  $x_{ij} \equiv x_i - x_j$ ). The separation length is  $\ell_0 = x_{32}$  and therefore  $\ell_1 + \ell_2 + \ell_0 = x_{41}$ .

The transition of the holographic mutual information for  $\text{AdS}_3$  has been studied in [14]. Introducing the harmonic ratio for the four extrema of the two intervals

$$x \equiv \frac{x_{12} x_{34}}{x_{13} x_{24}} = \frac{\ell_1 \ell_2}{(\ell_1 + \ell_0)(\ell_2 + \ell_0)} \tag{3.4}$$

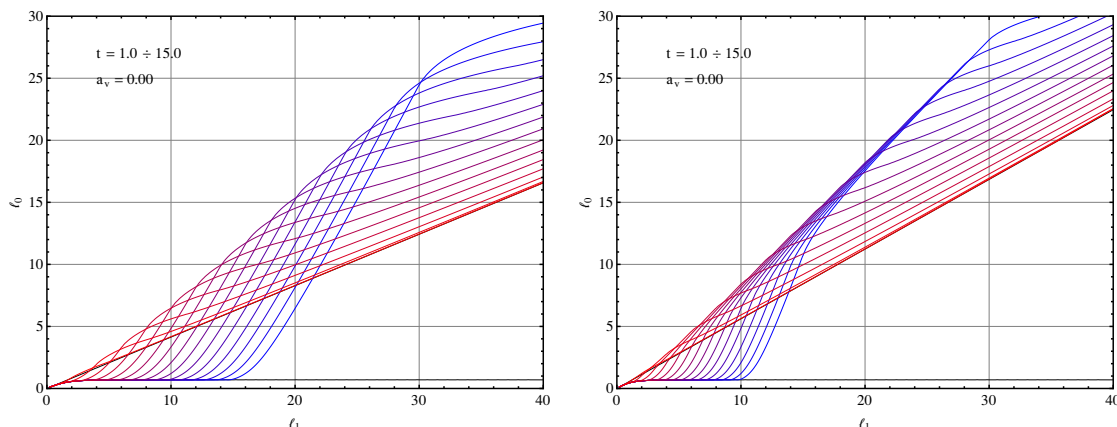


**Figure 9.** Transition point of the holographic mutual information  $I(\ell_0, \ell_1, \omega \ell_1)$  in the configuration space  $(\ell_1, \ell_0)$  for the three dimensional Vaidya metric in the thin shell limit. The analytic solution allows to extend the range of the parameters (see also figure 8). We give the curves for different boundary times which increase from the red to the blue curve. On the left we set  $\omega = 1$  while on the right  $\omega = 2$ . The curve above which the holographic mutual information vanishes for any boundary time depends on  $\omega$ .

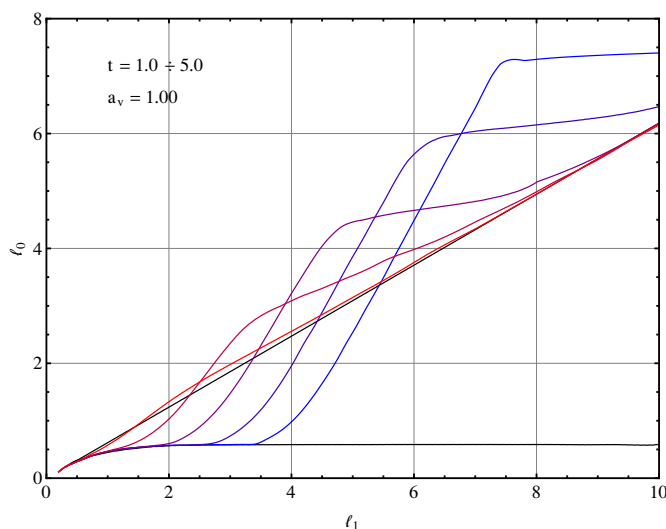


**Figure 10.** Transition point of the holographic mutual information  $I(\ell_0, \ell_1, \ell_1)$  for the four dimensional Vaidya metric in the configuration space  $(\ell_1, \ell_0)$  at different boundary times which increase going from the red to the blue curve. The black curves represent the limiting regimes of  $\text{AdS}_4$  (top curve) and Schwarzschild black hole (bottom curve). Also in four dimensions there is a curve above which the holographic mutual information is zero for any boundary time.

and employing the first formula in (2.24), the holographic mutual information of two disjoint intervals for  $\text{AdS}_3$  reads [14]

$$I(A_1, A_2) = \begin{cases} 0 & x < 1/2 \\ \frac{c}{3} \log \left( \frac{\ell_1 \ell_2}{\ell_0 (\ell_1 + \ell_2 + \ell_0)} \right) = \frac{c}{3} \log \left( \frac{x}{1-x} \right) & x > 1/2 \end{cases} \quad (3.5)$$

where we recall that  $c = 3l/(2G_N^{(3)})$  [56]. The transition point  $x = 1/2$  corresponds to the solution of  $l_1 l_2 / [\ell_0(l_1 + l_2 + \ell_0)] = 1$ , namely when the argument of the logarithm in (3.5) is equal to 1. Parameterizing  $l_2$  as  $l_2 = \omega l_1$  with  $\omega > 0$ , the equation  $x = 1/2$  becomes a second order equation for  $\ell_0$  (see (3.4)) with only one positive solution

$$\ell_0 = \frac{1 + \omega}{2} \left( \sqrt{\frac{4\omega}{(1 + \omega)^2} + 1} - 1 \right) \ell_1. \tag{3.6}$$

This curve is a line in the plane  $(\ell_1, \ell_0)$  passing through the origin whose angular coefficient depends on  $\omega$ . For  $\omega = 1$  it becomes  $\ell_0 = (\sqrt{2} - 1)\ell_1$  and this case is displayed in figure 8 and 9 (plot on the left). In plot on the right of figure 9 we set  $\omega = 2$ .

The limiting regime at late times is the BTZ black hole. By employing the second formula in (2.24), one finds that the equation (3.3) for the transition curve in the configuration space given by  $l_2, l_1$  and  $\ell_0$  can be written as follows

$$\frac{\sinh(\pi l_1 / \beta_H) \sinh(\pi l_2 / \beta_H)}{\sinh(\pi \ell_0 / \beta_H) \sinh(\pi(l_1 + l_2 + \ell_0) / \beta_H)} = 1. \tag{3.7}$$

Introducing  $\omega$  through  $l_2 = \omega l_1$  as above and using the addition formulas for the hyperbolic functions, the equation (3.7) becomes

$$\sinh^2 \left( \frac{\pi \ell_0}{\beta_H} \right) \left[ B(\ell_1, \omega) + C(\ell_1, \omega) \coth \left( \frac{\pi \ell_0}{\beta_H} \right) \right] = 1 \tag{3.8}$$

where we have defined

$$B(\ell_1, \omega) \equiv \coth \left( \frac{\pi \ell_1}{\beta_H} \right) \coth \left( \frac{\pi \omega \ell_1}{\beta_H} \right) + 1 \quad C(\ell_1, \omega) \equiv \coth \left( \frac{\pi \ell_1}{\beta_H} \right) + \coth \left( \frac{\pi \omega \ell_1}{\beta_H} \right). \tag{3.9}$$

Expressing the hyperbolic functions in their exponential form, the equation (3.8) becomes a second order equation in terms of  $e^{2\pi \ell_0 / \beta_H}$  and its positive root provides  $\ell_0$  in terms of  $\ell_1$  and  $\omega$ . The result reads

$$\ell_0 = \frac{\beta_H}{2\pi} \log \left( \frac{B(\ell_1, \omega) + 2 + \sqrt{4[1 + B(\ell_1, \omega)] + C(\ell_1, \omega)^2}}{B(\ell_1, \omega) + C(\ell_1, \omega)} \right). \tag{3.10}$$

In figure 8 and 9 this curve is the black one below all other. The curve (3.10) passes through the origin  $(\ell_1, \ell_0) = (0, 0)$  and it always stays below the line (3.6). Moreover, the line (3.6) is tangent to (3.10) at the origin and this provides a check of (3.10) because for small  $\ell_1$  and finite  $\omega$  (which implies small  $l_2$  as well) the minimal curves remain close to the boundary and therefore only the asymptotic geometry of BTZ, which is  $AdS_3$ , matters. For any finite  $\omega > 0$ , the curve (3.10) tends asymptotically to a horizontal line  $\ell_0 = \tilde{\ell}_0$  when  $\ell_1$  is large. In this limit both disjoint interval are large while the ratio between them, being given by  $\omega$ , is kept fixed. Quantitatively, since for  $\ell_1 \rightarrow +\infty$  we have  $B(\ell_1, \omega) \rightarrow 2$  and  $C(\ell_1, \omega) \rightarrow 2$ , the asymptotic value  $\tilde{\ell}_0$  reads

$$\tilde{\ell}_0 = \frac{\beta_H}{\pi} \log \sqrt{2} \tag{3.11}$$

and it is independent of  $\omega$ . This means that in the BTZ background, when the separation  $\ell_0$  is larger than  $\tilde{\ell}_0$ , the holographic mutual information is zero for any  $\ell_1$  and  $l_2$ .

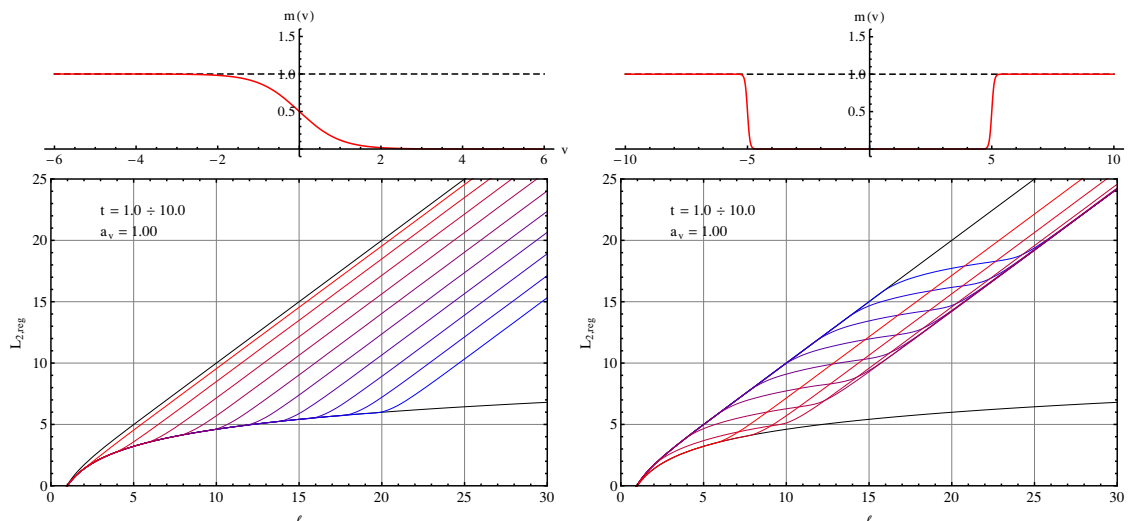


**Figure 11.** Regularized length  $L_{\text{reg}}$  for three dimensional Vaidya metric when the null energy condition is violated: a change of concavity is manifest in both cases. The mass profiles used are shown above and they are  $m(v) = \frac{M}{2} [2 + \tanh((v - v_0/2)/a_v) - \tanh((v + v_0/2)/a_v)]$  on the right and  $m(v) = \frac{M}{2} [1 - \tanh(v/a_v)]$  on the left, with  $M = 1$ ,  $a_v = 0.1$ ,  $v_0 = 10$ .

#### 4 Strong subadditivity and null energy condition

In this section we explore the relation between the null energy condition for the Vaidya metrics and the strong subadditivity condition, which is an important inequality satisfied by the entanglement entropy. We find that a violation of the null energy condition leads to a violation of strong subadditivity.<sup>2</sup>

Consider a quantum system that is partitioned into three or more subsystems, i.e. its Hilbert space  $H$  can be written as  $H = \otimes_i H_i$ , and let us denote by  $\rho_{i_1, i_2, \dots}$  the reduced density matrix obtained by tracing the full density matrix of the system over all  $H_j$  with  $j \neq i_1, i_2, \dots$ . It can be shown, on very general grounds, that the Von Neumann entropy satisfies the *subadditivity condition*

$$S(\rho_1) + S(\rho_2) \geq S(\rho_{1,2}) \tag{4.1}$$

and also the following two inequalities

$$\begin{aligned} S(\rho_{1,2}) + S(\rho_{2,3}) &\geq S(\rho_2) + S(\rho_{1,2,3}) \\ S(\rho_{1,2}) + S(\rho_{2,3}) &\geq S(\rho_1) + S(\rho_3) \end{aligned} \tag{4.2}$$

which are equivalent and known as *strong subadditivity condition* (see [11, 12, 57] and the refs therein for more detailed discussions).

---

<sup>2</sup>We remark that this result has been independently obtained also by Robert Callan and Matthew Headrick.

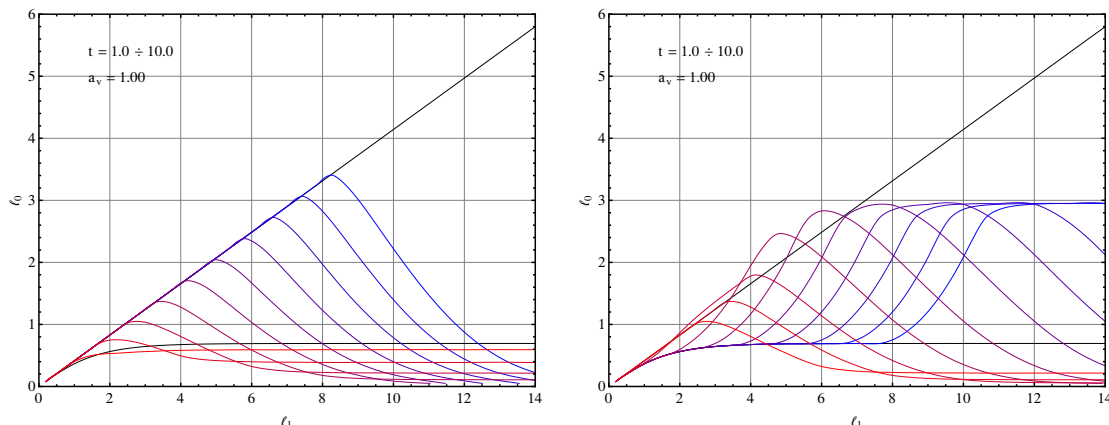


**Figure 12.** Location of the transition point of  $I(\ell_0, \ell_1, \ell_1)$  when the null energy condition is violated: the curve is not monotonically increasing with  $\ell_1$ . The mass profiles employed in the plots are the same as in figure 11.

If the Hilbert space is partitioned into the product of the Hilbert spaces of local degrees of freedom belonging to non intersecting regions of space  $A_1, A_2, \dots$ , the inequalities (4.1) and (4.2) can be written respectively as

$$S_{A_1} + S_{A_2} \geq S_{A_2 \cup A_2} \tag{4.3}$$

and

$$\begin{aligned} S_{A_1 \cup A_2} + S_{A_2 \cup A_3} &\geq S_{A_2} + S_{A_1 \cup A_2 \cup A_3} \\ S_{A_1 \cup A_2} + S_{A_2 \cup A_3} &\geq S_{A_1} + S_{A_3} . \end{aligned} \tag{4.4}$$

In one dimensional systems (or when the symmetry of the regions considered is such that the problem is effectively one-dimensional), for a complete description, it is sufficient to consider the entanglement entropy of an interval as a function of its length  $\ell$ , and the two inequalities of the strong subadditivity are more conveniently expressed in terms of the function  $S(\ell)$ . The first inequality in (4.4) states that the function  $S(\ell)$  is concave, and the second that it is non decreasing.

In section 2.1 we mentioned (see (2.10)) that for the Vaidya metrics (2.1) the condition  $m'(v) \geq 0$  guarantees that the null energy condition is satisfied. By choosing a mass function that does not monotonically increase with  $v$ , we can violate the null energy condition and explore the consequences of this violation on the entanglement entropy. The results are shown in figure 11 and 12.

The curves in figure 11 are not concave functions of  $\ell$ , but they are still non-decreasing. Therefore only the first of the two inequalities is violated. This means that they cannot be equivalent in this setting. In order to clarify this apparent contradiction we have to discuss how the equivalence between the inequalities is proven, both in quantum mechanics and holographically.

The two inequalities can be shown to be equivalent by introducing an auxiliary fourth Hilbert space  $H_4$  such that  $\rho_{1,2,3} = \text{Tr}_4 |\psi\rangle\langle\psi|$ , for a certain pure state  $|\psi\rangle$  [57]. Then

$$S(\rho_{1,2,4}) = S(\rho_3) \quad \text{and} \quad S(\rho_{1,4}) = S(\rho_{2,3}) \tag{4.5}$$

and hence, if we write the first inequality for  $3 \leftrightarrow 4$ ,  $1 \leftrightarrow 2$

$$S(\rho_{1,2}) + S(\rho_{1,4}) \geq S(\rho_1) + S(\rho_{1,2,4}) \tag{4.6}$$

and substitute, we get the second, and viceversa.

If one tries to replicate the argument above in the holographic setting, one encounters a difficulty because, although we are guaranteed that it is always possible to find the Hilbert space  $H_4$ , it is not guaranteed that it will be the Hilbert space of the local degrees of freedom of some other region of the boundary theory. However, that is the only known kind of partitioning of the Hilbert space that allows for a holographic computation. It turns out that, if the bulk manifold is homologous to the boundary, the problem is easily solved:  $H_4$  can be taken to be the Hilbert space of the degrees of freedom of the region  $A_4 = \overline{A_1 \cup A_2 \cup A_3}$ , the complement of  $A_1 \cup A_2 \cup A_3$ , because it satisfies

$$S_{A_1 \cup A_2 \cup A_4} = S_{A_3} \quad \text{and} \quad S_{A_1 \cup A_4} = S_{A_2 \cup A_3} \tag{4.7}$$

which are the equivalent of (4.6).

On the other hand, if the manifold contains a black hole, the problem is more complicated, because the entropy of the entire system is non-zero, and hence (4.7) do not hold. One has to rely on the conjecture that the holographic entanglement entropy is actually describing the entanglement entropy of a certain quantum system, and hence on the quantum information proof mentioned above. If the dual geometry is sufficiently unphysical, as is the case for when the null energy condition is violated, it may not be the holographic description of any quantum system, and there is no a priori reason to expect that the two inequalities should be equivalent.

In terms of the mutual information  $I(A_1, A_2)$  for two disjoint regions (3.1) the subadditivity inequality (4.3) implies that

$$I(A_1, A_2) \geq 0 \tag{4.8}$$

while the first strong subadditivity inequality (4.4) can be written as follows

$$I(A_1, A_2 \cup A_3) \geq I(A_1, A_2) \tag{4.9}$$

i.e., the mutual information increases as one of the two regions is enlarged while the other one is kept fixed. Applying this inequality twice, we can also conclude that when two equal regions are enlarged by the same quantity, the mutual information increases.

From the transition curves in figure 12, we can observe that the holographic mutual information is not monotonically increasing with  $\ell_1$ . This behavior is another manifestation of the violation of the first strong subadditivity inequality, and has to be contrasted with figure 8 discussed in the previous section, where we used the mass profile (2.9) (figure 1) and the null energy condition is satisfied.

## 5 Holographic tripartite information and monogamy

In this section we consider the holographic tripartite information for three dimensional Vaidya metrics and show that the monogamy of the holographic mutual information is violated when the null energy condition is not satisfied.

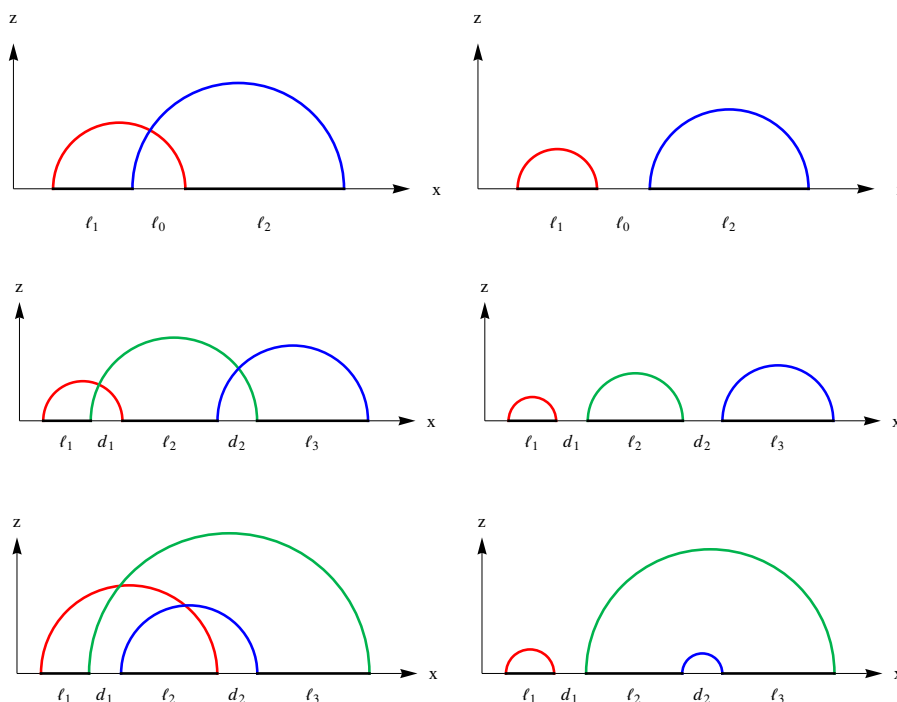


**Figure 13.** Schematic representations of some mixed configurations occurring in the computation of  $S_{A_1 \cup A_2}$  (upper line) and  $S_{A_1 \cup A_2 \cup A_3}$  (middle and bottom line). If the regularized area of the surface homologous to a single region  $A$  is an increasing function of the size of  $A$ , then the configuration on the left is suboptimal w.r.t. the one on the right (each line on the left should be compared with the one on the right having the same color) and thus it does not occur in the holographic mutual information or the holographic tripartite information.

In addition to the mutual information, another interesting quantity that can be defined from the entanglement entropy is the *tripartite information*

$$I_3(A_1, A_2, A_3) \equiv S_{A_1} + S_{A_2} + S_{A_3} - S_{A_1 \cup A_2} - S_{A_1 \cup A_3} - S_{A_2 \cup A_3} + S_{A_1 \cup A_2 \cup A_3} \quad (5.1)$$

where  $A_1$ ,  $A_2$  and  $A_3$  are disjoint regions. In contrast with the mutual information, this quantity is free of divergences even when the regions share their boundary. It is a measure of the extensivity of the mutual information; indeed, the definition (5.1) can be also written as

$$I_3(A_1, A_2, A_3) \equiv I(A_1, A_2) + I(A_1, A_3) - I(A_1, A_2 \cup A_3). \quad (5.2)$$

Thus, the mutual information is extensive when  $I_3 = 0$ , superextensive when  $I_3 < 0$  and subextensive when  $I_3 > 0$ . In particular, in either the extensive or the superextensive case, namely

$$I(A_1, A_2) + I(A_1, A_3) \leq I(A_1, A_2 \cup A_3) \quad (5.3)$$

the mutual information is said to be monogamous. For a generic quantum system, the tripartite information can be positive, negative or zero, depending on the choice of the regions.

Recently it has been shown [12] that for quantum systems with a holographic dual the tripartite information is always monogamous. As for the strong subadditivity condition, the



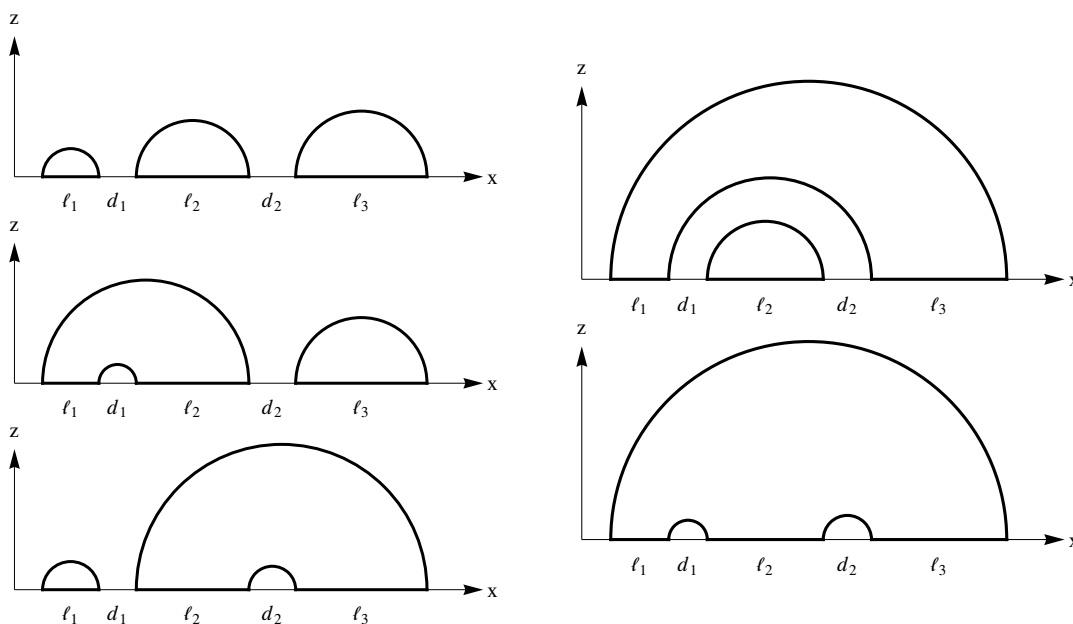


**Figure 14.** Schematic geodesics configurations to consider in the computation of  $S_{A_1 \cup A_2 \cup A_3}$ .

proof only holds in the case of static dual geometries because in dynamical backgrounds it is not always guaranteed that the surfaces involved in the mixed configurations intersect each other. It is therefore interesting to explore the behavior of the holographic tripartite information in the simple dynamical backgrounds like the three dimensional Vaidya geometries.

Among the terms occurring in the definition of the holographic tripartite information, the computation of  $S_{A_1 \cup A_2 \cup A_3}$  deserves a short discussion. In one spatial dimension the three regions are just intervals, and, according to prescription of [8] for dynamical backgrounds, one has to find the extremal set of geodesics connecting all the extrema of the intervals. In principle, in presence of  $N$  intervals one should compare  $(2N - 1)!!$  configurations (15 in our case). However, since  $L_{2,\text{reg}}(\ell)$  at fixed time is an increasing function of  $\ell$ , for  $N = 3$  we are left only with the five configurations shown in figure 14, by the argument sketched in figure 13. Thus,  $S_{A_1 \cup A_2 \cup A_3}$  is given by the minimum among the following quantities

$$\begin{array}{l}
 S(\ell_1) + S(\ell_2) + S(\ell_3) \\
 S(\ell_1 + d_2 + \ell_2) + S(d_1) + S(\ell_3) \\
 S(\ell_1) + S(\ell_2 + d_2 + \ell_3) + S(d_2) \\
 S(\ell_1 + d_1 + \ell_2 + d_2 + \ell_3) + S(d_1 + \ell_2 + d_2) + S(\ell_2) \\
 S(\ell_1 + d_1 + \ell_2 + d_2 + \ell_3) + S(d_2) + S(d_2)
 \end{array}
 \left. \begin{array}{l}
 \\
 \\
 \\
 \\
 \end{array} \right\}
 \begin{array}{l}
 \text{three disconnected volumes} \\
 \text{two disconnected volumes} \\
 \text{one connected volume.}
 \end{array}
 \tag{5.4}$$

Figure 15 displays the time dependence of the tripartite information when the intervals have the same size  $\ell_1 = \ell_2 = \ell_3 = 5$  and are separated by the same amount  $d_1 = d_2 = \ell_0$ , with several values of  $\ell_0$  shown. The behavior is quite complicated and involves different

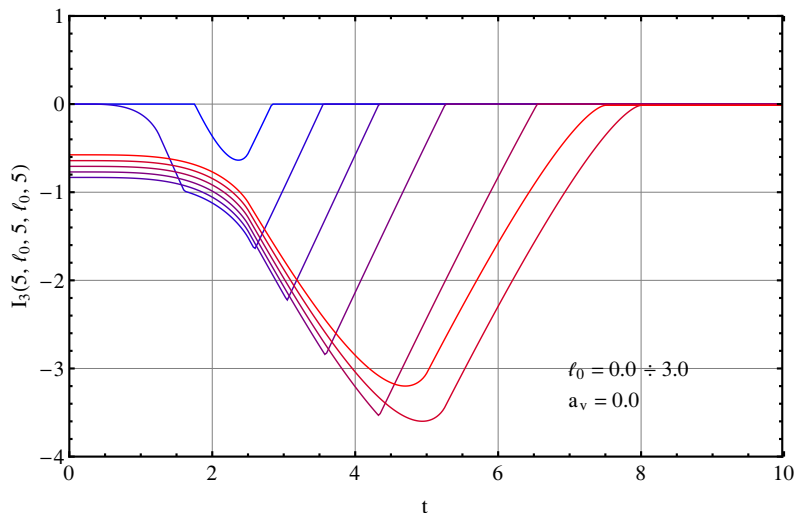


**Figure 15.** Time evolution of the tripartite information for the three dimensional ( $d = 2$ ) Vaidya geometry in the thin shell limit. The three intervals have the same size  $\ell_1 = \ell_2 = \ell_3 = 5$  and are separated by the same distance  $d_1 = d_2 = \ell_0$ . The plot shows that the holographic mutual information is always monogamous.

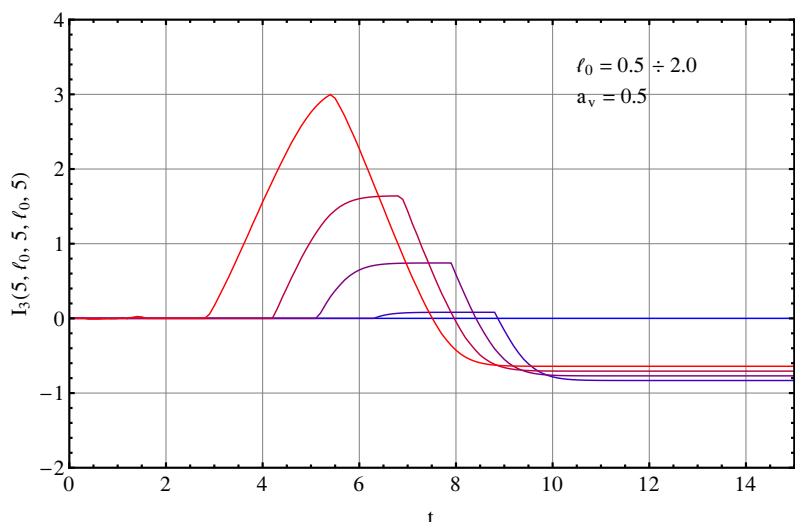


**Figure 16.** Time evolution of the tripartite information for the three dimensional ( $d = 2$ ) Vaidya geometry when the null energy condition is violated: the mass function decreases from  $m(-\infty) = 1$  to  $m(+\infty) = 0$ , according to the profile shown in figure 11. Since  $I_3$  becomes positive for certain range of  $t$ , the monogamy of the holographic mutual information is violated.

regimes, but the quantity is always non positive, even though the geometry is not static. At late times all curves go to zero, meaning that, in the thermal state dual to the BTZ black hole, the holographic mutual information is extensive.

Given the results of section 4 about the relation between the strong subadditivity of the holographic entanglement entropy and the null energy condition, we can explore the possible relation between the monogamy of the holographic mutual information and the

null energy condition in the same way, namely by employing mass profiles  $m(v)$  which have  $m'(v) < 0$  for some range of  $v$ . This is relevant because the strong subadditivity and the monogamy are independent conditions. In figure 16 we show the time evolution of the holographic tripartite information with the same interval configuration of figure 15 but with the mass function  $m(v)$  decreasing from  $M = 1$  at early times ( $v \rightarrow -\infty$ ) to  $M = 0$  at late times ( $v \rightarrow +\infty$ ) according to the profile shown in figure 11 (plot on the left). The holographic tripartite information becomes positive for certain ranges of  $t$ , telling us that a violation of the null energy condition leads to a non monogamous holographic mutual information.

## 6 Conclusions

We studied the holographic mutual information for dynamical backgrounds given by the Vaidya metrics in three and four dimensions. We found that it is non monotonic as function of the boundary time and its behavior depends on the configuration of the two disjoint regions.

From the transition curves of the holographic mutual information in the configuration space we could identify different behaviors and also find a region in the configuration space where the holographic mutual information is zero at all times. Considering the holographic tripartite information, we observed that the holographic mutual information is monogamous also for these time dependent backgrounds in the ranges of the variables explored.

By modifying the mass profile occurring in the Vaidya metrics, we showed that the null energy condition is a necessary condition both for the strong subadditivity of the holographic entanglement entropy and for the monogamy of the holographic mutual information. A deeper understanding of the relation between the null energy condition and the inequalities satisfied by the quantities defined from the holographic entanglement entropy is needed.

## Acknowledgments

We acknowledge Francesco Bigazzi, John Cardy, Pasquale Calabrese, Horatio Casini, Mark Mueller, Andrea Sportiello and Tadashi Takayanagi for stimulating discussions. We are grateful in particular to Matthew Headrick and John McGreevy for helpful conversations and comments.

ET acknowledges the organizers of the Aspen workshop *Quantum Information in Quantum Gravity and Condensed Matter Physics* and also Pisa University and the Institute Henri Poincaré for the warm hospitality during parts of this work. ET is supported by Istituto Nazionale di Fisica Nucleare (INFN) through the “Bruno Rossi” fellowship. AA and ET are supported by funds of the U.S. Department of Energy under the cooperative research agreement DE-FG02-05ER41360.

## References

- [1] M. Srednicki, *Entropy and area*, *Phys. Rev. Lett.* **71** (1993) 666 [[hep-th/9303048](#)] [[INSPIRE](#)].
- [2] C.G. Callan Jr. and F. Wilczek, *On geometric entropy*, *Phys. Lett. B* **333** (1994) 55 [[hep-th/9401072](#)] [[INSPIRE](#)].
- [3] C. Holzhey, F. Larsen and F. Wilczek, *Geometric and renormalized entropy in conformal field theory*, *Nucl. Phys. B* **424** (1994) 443 [[hep-th/9403108](#)] [[INSPIRE](#)].
- [4] P. Calabrese and J.L. Cardy, *Entanglement entropy and quantum field theory*, *J. Stat. Mech.* **0406** (2004) P06002 [[hep-th/0405152](#)] [[INSPIRE](#)].
- [5] P. Calabrese and J. Cardy, *Entanglement entropy and conformal field theory*, *J. Phys. A* **A 42** (2009) 504005 [[arXiv:0905.4013](#)] [[INSPIRE](#)].
- [6] S. Ryu and T. Takayanagi, *Holographic derivation of entanglement entropy from AdS/CFT*, *Phys. Rev. Lett.* **96** (2006) 181602 [[hep-th/0603001](#)] [[INSPIRE](#)].
- [7] S. Ryu and T. Takayanagi, *Aspects of holographic entanglement entropy*, *JHEP* **08** (2006) 045 [[hep-th/0605073](#)] [[INSPIRE](#)].
- [8] V.E. Hubeny, M. Rangamani and T. Takayanagi, *A covariant holographic entanglement entropy proposal*, *JHEP* **07** (2007) 062 [[arXiv:0705.0016](#)] [[INSPIRE](#)].
- [9] T. Nishioka, S. Ryu and T. Takayanagi, *Holographic entanglement entropy: an overview*, *J. Phys. A* **A 42** (2009) 504008 [[arXiv:0905.0932](#)] [[INSPIRE](#)].
- [10] T. Hirata and T. Takayanagi, *AdS/CFT and strong subadditivity of entanglement entropy*, *JHEP* **02** (2007) 042 [[hep-th/0608213](#)] [[INSPIRE](#)].
- [11] M. Headrick and T. Takayanagi, *A holographic proof of the strong subadditivity of entanglement entropy*, *Phys. Rev. D* **76** (2007) 106013 [[arXiv:0704.3719](#)] [[INSPIRE](#)].
- [12] P. Hayden, M. Headrick and A. Maloney, *Holographic mutual information is monogamous*, [arXiv:1107.2940](#) [[INSPIRE](#)].
- [13] D.V. Fursaev, *Proof of the holographic formula for entanglement entropy*, *Journal of High Energy Physics* **9** (2006) 18 [[arXiv:hep-th/0606184](#)].
- [14] M. Headrick, *Entanglement Renyi entropies in holographic theories*, *Phys. Rev. D* **82** (2010) 126010 [[arXiv:1006.0047](#)] [[INSPIRE](#)].
- [15] M. Caraglio and F. Gliozzi, *Entanglement entropy and twist fields*, *JHEP* **11** (2008) 076 [[arXiv:0808.4094](#)] [[INSPIRE](#)].
- [16] S. Furukawa, V. Pasquier and J. Shiraishi, *Mutual information and compactification radius in a  $c = 1$  critical phase in one dimension*, *Phys. Rev. Lett.* **102** (2009) 170602 [[arXiv:0809.5113](#)] [[INSPIRE](#)].
- [17] P. Calabrese, J. Cardy and E. Tonni, *Entanglement entropy of two disjoint intervals in conformal field theory*, *J. Stat. Mech.* **0911** (2009) P11001 [[arXiv:0905.2069](#)] [[INSPIRE](#)].
- [18] P. Calabrese, J. Cardy and E. Tonni, *Entanglement entropy of two disjoint intervals in conformal field theory II*, *J. Stat. Mech.* **1101** (2011) P01021 [[arXiv:1011.5482](#)] [[INSPIRE](#)].
- [19] V. Alba, L. Tagliacozzo and P. Calabrese, *Entanglement entropy of two disjoint blocks in critical Ising models*, [arXiv:0910.0706](#) [[INSPIRE](#)].
- [20] M. Fagotti and P. Calabrese, *Entanglement entropy of two disjoint blocks in XY chains*, *J. Stat. Mech.* **1004** (2010) P04016 [[arXiv:1003.1110](#)] [[INSPIRE](#)].

- [21] M. Fagotti and P. Calabrese, *Universal parity effects in the entanglement entropy of XX chains with open boundary conditions*, *J. Stat. Mech.* **1101** (2011) P01017 [[arXiv:1010.5796](#)] [[INSPIRE](#)].
- [22] V. Alba, L. Tagliacozzo and P. Calabrese, *Entanglement entropy of two disjoint intervals in  $c = 1$  theories*, *J. Stat. Mech.* **1106** (2011) P06012 [[arXiv:1103.3166](#)] [[INSPIRE](#)].
- [23] V.E. Hubeny and M. Rangamani, *Holographic entanglement entropy for disconnected regions*, *JHEP* **03** (2008) 006 [[arXiv:0711.4118](#)] [[INSPIRE](#)].
- [24] E. Tonni, *Holographic entanglement entropy: near horizon geometry and disconnected regions*, *JHEP* **05** (2011) 004 [[arXiv:1011.0166](#)] [[INSPIRE](#)].
- [25] P. Calabrese and J.L. Cardy, *Evolution of entanglement entropy in one-dimensional systems*, *J. Stat. Mech.* **0504** (2005) P04010 [[cond-mat/0503393](#)] [[INSPIRE](#)].
- [26] G. De Chiara, S. Montangero, P. Calabrese and R. Fazio, *Entanglement entropy dynamics in Heisenberg chains*, *J. Stat. Mech.* **0603** (2006) L03001 [[cond-mat/0512586](#)] [[INSPIRE](#)].
- [27] P. Calabrese and J.L. Cardy, *Time-dependence of correlation functions following a quantum quench*, *Phys. Rev. Lett.* **96** (2006) 136801 [[cond-mat/0601225](#)] [[INSPIRE](#)].
- [28] P. Calabrese and J. Cardy, *Quantum quenches in extended systems*, *J. Stat. Mech.* **0706** (2007) P06008 [[arXiv:0704.1880](#)] [[INSPIRE](#)].
- [29] P. Calabrese and J. Cardy, *Entanglement and correlation functions following a local quench: a conformal field theory approach*, *Journal of Statistical Mechanics: Theory and Experiment* **10** (2007) 4 [[arXiv:0708.3750](#)].
- [30] H. Diehl, *The theory of boundary critical phenomena*, *Int. J. Mod. Phys. B* **11** (1997) 3503 [[cond-mat/9610143](#)] [[INSPIRE](#)].
- [31] P. Calabrese and A. Gambassi, *Ageing properties of critical systems*, *J. Phys. A* **38** (2005) R133 [[cond-mat/0410357](#)] [[INSPIRE](#)].
- [32] V.E. Hubeny and M. Rangamani, *A holographic view on physics out of equilibrium*, *Adv. High Energy Phys.* **2010** (2010) 297916 [[arXiv:1006.3675](#)] [[INSPIRE](#)].
- [33] H. Stephani, D. Kramer, M. MacCallum, C. Hoenselaers and E. Herlt, *Exact solutions of Einstein's field equations*, Cambridge University Press, Cambridge U.K. (2003).
- [34] S.R. Das, T. Nishioka and T. Takayanagi, *Probe branes, time-dependent couplings and thermalization in AdS/CFT*, *JHEP* **07** (2010) 071 [[arXiv:1005.3348](#)] [[INSPIRE](#)].
- [35] P. Basu and S.R. Das, *Quantum quench across a holographic critical point*, [arXiv:1109.3909](#) [[INSPIRE](#)].
- [36] V.E. Hubeny, H. Liu and M. Rangamani, *Bulk-cone singularities & signatures of horizon formation in AdS/CFT*, *JHEP* **01** (2007) 009 [[hep-th/0610041](#)] [[INSPIRE](#)].
- [37] J. Abajo-Arrastia, J. Aparicio and E. Lopez, *Holographic evolution of entanglement entropy*, *JHEP* **11** (2010) 149 [[arXiv:1006.4090](#)] [[INSPIRE](#)].
- [38] T. Albash and C.V. Johnson, *Evolution of holographic entanglement entropy after thermal and electromagnetic quenches*, *New J. Phys.* **13** (2011) 045017 [[arXiv:1008.3027](#)] [[INSPIRE](#)].
- [39] S. Lin and E. Shuryak, *Toward the AdS/CFT gravity dual for high energy collisions. 3. Gravitationally collapsing shell and quasiequilibrium*, *Phys. Rev. D* **78** (2008) 125018 [[arXiv:0808.0910](#)] [[INSPIRE](#)].

- [40] S. Bhattacharyya and S. Minwalla, *Weak field black hole formation in asymptotically AdS spacetimes*, *JHEP* **09** (2009) 034 [[arXiv:0904.0464](#)] [[INSPIRE](#)].
- [41] V. Balasubramanian, A. Bernamonti, J. de Boer, N. Copland, B. Craps, et al., *Thermalization of strongly coupled field theories*, *Phys. Rev. Lett.* **106** (2011) 191601 [[arXiv:1012.4753](#)] [[INSPIRE](#)].
- [42] V. Balasubramanian, A. Bernamonti, J. de Boer, N. Copland, B. Craps, et al., *Holographic thermalization*, *Phys. Rev. D* **84** (2011) 026010 [[arXiv:1103.2683](#)] [[INSPIRE](#)].
- [43] J. Aparicio and E. Lopez, *Evolution of two-point functions from holography*, *JHEP* **12** (2011) 082 [[arXiv:1109.3571](#)] [[INSPIRE](#)].
- [44] V. Balasubramanian, A. Bernamonti, N. Copland, B. Craps and F. Galli, *Thermalization of mutual and tripartite information in strongly coupled two dimensional conformal field theories*, *Phys. Rev. D* **84** (2011) 105017 [[arXiv:1110.0488](#)] [[INSPIRE](#)].
- [45] S.W. Hawking and G.F.R. Ellis, *The large scale structure of space-time*, Cambridge University Press, Cambridge U.K. (1973).
- [46] R.M. Wald, *General relativity*, The University of Chicago Press, Chicago U.S.A. and London U.K. (1984).
- [47] I. Booth, *Black hole boundaries*, *Can. J. Phys.* **83** (2005) 1073 [[gr-qc/0508107](#)] [[INSPIRE](#)].
- [48] D. Freedman, S. Gubser, K. Pilch and N. Warner, *Renormalization group flows from holography supersymmetry and a c theorem*, *Adv. Theor. Math. Phys.* **3** (1999) 363 [[hep-th/9904017](#)] [[INSPIRE](#)].
- [49] R.C. Myers and A. Sinha, *Holographic c-theorems in arbitrary dimensions*, *JHEP* **01** (2011) 125 [[arXiv:1011.5819](#)] [[INSPIRE](#)].
- [50] I. Affleck and A.W. Ludwig, *Universal noninteger ‘ground state degeneracy’ in critical quantum systems*, *Phys. Rev. Lett.* **67** (1991) 161 [[INSPIRE](#)].
- [51] A. Karch and L. Randall, *Locally localized gravity*, *JHEP* **05** (2001) 008 [[hep-th/0011156](#)] [[INSPIRE](#)].
- [52] T. Takayanagi, *Holographic dual of BCFT*, *Phys. Rev. Lett.* **107** (2011) 101602 [[arXiv:1105.5165](#)] [[INSPIRE](#)].
- [53] M. Fujita, T. Takayanagi and E. Tonni, *Aspects of AdS/BCFT*, *JHEP* **11** (2011) 043 [[arXiv:1108.5152](#)] [[INSPIRE](#)].
- [54] J.L. Barbon and C.A. Fuertes, *A note on the extensivity of the holographic entanglement entropy*, *JHEP* **05** (2008) 053 [[arXiv:0801.2153](#)] [[INSPIRE](#)].
- [55] M. Bañados, C. Teitelboim and J. Zanelli, *The black hole in three-dimensional space-time*, *Phys. Rev. Lett.* **69** (1992) 1849 [[hep-th/9204099](#)] [[INSPIRE](#)].
- [56] J. Brown and M. Henneaux, *Central charges in the canonical realization of asymptotic symmetries: an example from three-dimensional gravity*, *Commun. Math. Phys.* **104** (1986) 207 [[INSPIRE](#)].
- [57] M.A. Nielsen, I.L. Chuang, *Quantum computation and quantum information*, Cambridge University Press, Cambridge U.K. (2000).